Volume loss, fluid flow, and coaxial versus noncoaxial deformation in retrograde, amphibolite facies shear zones, northern Malawi, east-central Africa

Uwe Ring* *Institut für Geowissenschaften, Johannes Gutenberg-Universität, Becherweg 21, 55099 Mainz, Germany*

ABSTRACT

Two retrograde, amphibolite facies shear zones were studied to explore the relationship between retrograde mineral reactions, volume strain, fluid flow, mylonitization, and coaxial versus noncoaxial deformation. The two shear zones are the contractional Mafwewu Hills shear zone and the transcurrently displacing Mkamasa River shear zone of northern Malawi. In general, shear-zone formation is characterized by the breakdown of feldspar and biotite and the formation of sillimanite, quartz, and water. Silica, alkali, and alkali earth elements were mobile. Mass-balance calculations, based on major- and trace-element geochemistry, indicate as much as 50%–60% volume loss in mylonite. Fluid to rock ratios estimated from the calculated depletions of silica are as much as 200–400, indicating that the initiation and activity of the shear zones were accompanied by large amounts of fluids that infiltrated the shear zones. These fluids caused an almost complete loss of alkalies within the shear zone, leading to the development of almost "dry" and sheet-silicate–free mylonite. It is proposed that the associated destabilization of micas destroyed the pathways for fluid circulation and ultimately caused the cessation of shearing.

In the Mafwewu Hills shear zone, shear-zone–related stretching lineations are oriented parallel to tectonic transport. In the Mkamasa River shear zone, the stretching lineations curve from a subhorizontal attitude in the wall rock into a subvertical attitude in mylonite characterized by large volume loss. Shear bands in the Mkamasa River shear zone indicate a sinistral sense of shear. A synoptic analysis of mesoscale S and Z asymmetric folds indicates that the orientation of the stretching lineations in mylonite characterized by large volume loss is subperpendicular to the regional tectonic transport direction. Aspect ratios of feldspar and quartz in XZ sections ($X \geq Y \geq Z$, principal axes of finite-strain ellipsoid) show oblate grain shapes and show a positive correlation with volume strain. Mean kinematic vorticity numbers are 0.26–0.44 in the wall rock and 0.57–0.79 in mylonite. In mylonite, small kinematic vorticity numbers correlate with large volume loss. The transport-perpendicular orientation of the stretching lineations in strongly volume-deficient mylonite is thought to be the result of a pronounced component of shortening normal to the shear zone; the resulting higher degree of coaxial deformation controlled the final orientation of the stretching lineations.

INTRODUCTION

Retrograde shear zones are ubiquitous features in continental basement complexes and are associated with the excavation of metamorphic terrains. They are sites of enhanced metamorphic reactions (e.g., White and Knipe, 1978) and conduits through which large quantities of crustal fluids circulate. Therefore, retrograde shear zones are considered a fundamental feature of metamorphic flow patterns (e.g., Etheridge, 1983). Retrograde shear zones are commonly characterized by water-absorbing mineral reactions. In some circumstances, however, retrograde metamorphic reactions may cause the discharge of water. Such reactions include the formation of sillimanite and quartz from biotite and feldspar (Zwart, 1965; Losert, 1968) and have been described from shear zones in the high-grade basement of the Black Forest of southwestern Germany (Flöttmann, 1988). Water-releasing retrograde reactions may have important consequences for the deformational behavior of the crust because the liberated water may have an influence on deformation processes (Hubbert and Ruby, 1959). However, a critical question is how much fluid these reactions contribute to the total fluid budget in a shear zone.

Midcrustal shear zones are commonly associated with profound changes in chemical composition that reflect extensive fluid infiltration usually causing large volume losses of as much as 60%–70% (O'Hara, 1988, 1994; Flöttmann, 1988; Selverstone et al., 1991). This volume loss implies that strain in those shear zones did not accumulate by progressive simple shear. Nonsimple-shear zones may have considerable kinematic consequences; for example, in zones of transpression, where material can move laterally out of the profile plane, the maximum principal elongation may be the axis of the rotational component of deformation (Simpson and De Paor, 1993; Passchier, 1997) and a mineral lineation can develop orthogonal to tectonic transport (Passchier, 1987; Robin and Cruden, 1994).

In this article I present the results from a study of two retrograde shear zones (Fig. 1) that developed under amphibolite facies metamorphism in the Proterozoic crust of northern Malawi. The relationship between retrograde mineral reactions, mylonitization, volume loss, and structural development is investigated. The two retrograde shear zones are the contractional Mafwewu Hills shear zone and the transcurrently displacing Mkamasa River shear zone. I conclude that the formation of both shear zones was intimately associated with the crystallization of sillimanite and quartz from

*E-mail: ring@mail.uni-mainz.de.

Data Repository item 9912 contains additional material related to this article.

GSA Bulletin; January 1999; v. 111; no. 1; p. 123–142; 17 figures; 6 tables.

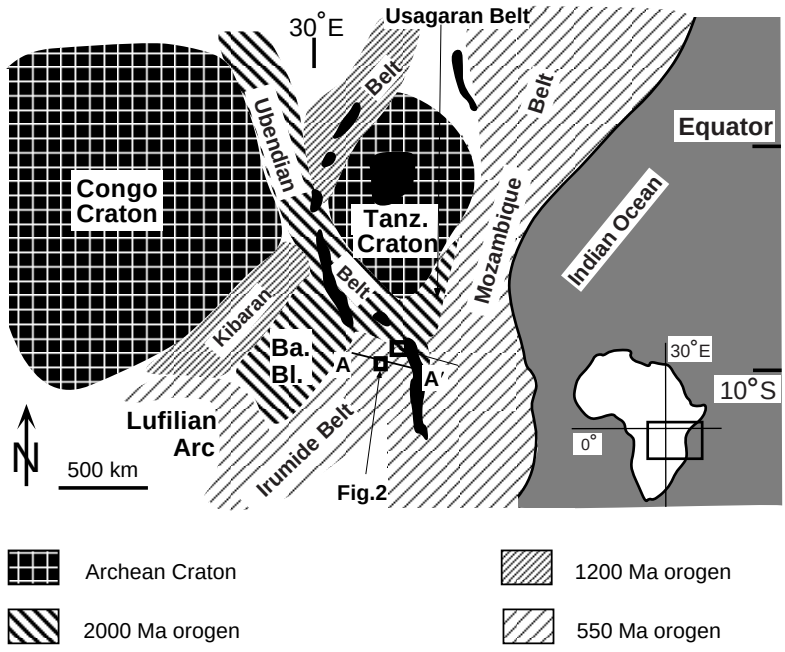

Figure 1. Distribution of mobile belts and cratons in east-central Africa (Ba.bl.—Bangweulu block). The studied shear zones are within the Ubendian and Irumide belts. The localities of the maps shown in Figures 2 and 3 are shown. Great African lakes are shown in black. Inset shows position of main map within Africa. Tanz—Tanzania.

biotite and feldspar. Deformation within the retrograde shear zones was characterized by large volume loss, high fluid/rock ratios, and an oblate strain geometry. In the Mafwewu Hills shear zone, stretching lineations still reflect the tectonic transport direction, whereas in strongly volume-deficient parts of the Mkamasa River shear zone, stretching lineations developed orthogonal to tectonic transport.

TECTONIC SETTING

The Proterozoic basement of northern Malawi is at the junction of three linear belts of crustal mobility, the Ubendian, the Irumide, and the Mozambique belts (Fig. 1). The basement was largely assembled during the ca. 2 Ga Ubendian orogeny (Dodson et al., 1975; Ring et al., 1997). The Pan-African orogeny occurred at the Proterozoic-Cambrian boundary and included large-scale, top-to-east-southeast–directed thrusts in the Irumide belt. Thrusting was concurrent with sinistral strike-slip shearing in the Mugesse shear zone, which developed within the Ubendian belt of northern Malawi. This contractional event proceeded under amphibolite facies metamorphic conditions (Ring, 1997).

The lithology of the basement is granitoid, partly migmatitic paragneiss and orthogneiss and granulite (e.g., Fitches, 1970). The paragneiss is a grayish to black gneiss with a marked schistosity that usually results from a metamorphic segregation into leucocratic and dark layers at the millimeter to centimeter scale. The major rock-forming minerals are quartz, biotite, feldspar, sillimanite, and garnet. Pinkish-gray metagranite and orthogneiss in general consist of feldspar, quartz, and biotite. The granulite contains cordierite, sillimanite, garnet, spinel, and potassium feldspar. Orthogneiss and paragneiss are interleaved with quartzite, the latter of which contains sillimanite and is characterized throughout northern Malawi by amphibolite facies metamorphic assemblages.

The regional geologic setting of the two studied retrograde shear zones is shown in Figures 2 and 3. The Mafwewu Hills shear zone (Fig. 2) developed in the Irumide belt. The wall rock is a medium-grained (2–3 mm) paragneiss that is interleaved with small amphibolite layers and lenses and is cut by a network of anastomosing, moderately west-dipping, top-to-east-southeast–displacing shear zones. Strike, dip, and dip direction of the shear zones may vary due to later open to tight folding. Close to the shear-zone boundaries, the paragneiss is generally protomylonitic and quartz veins are common. Two types of mylonite have been distinguished within the shear zone on the basis of changes in grain size, mineralogy and composition: (1) mylonite I, which is characterized by grain-size reduction and minor compositional changes, and (2) mylonite II, which shows pronounced grain-size reduction and a dramatic change in mineralogy and composition (Table 1). Shear-zone thickness varies along strike from a few meters to about 15 m. Locally pods of protomylonitic wall rock occur within the mylonite.

The Mkamasa River shear zone formed within the sinistrally displacing Mugesse shear zone (Fig. 3) and also developed in medium-grained (2–4 mm) paragneiss. The shear zone dips steeply (>75°) to the south-southwest and the strike varies from N10°E to N42°E. Based on the above criteria, mylonite I and mylonite II have also been distinguished (Table 2). In the west, the shear zone varies in width from 3 m to almost 10 m over a distance of ~1 km. In this area, a variably thick zone of mylonite II is developed within the center of the shear zone (Fig. 3B). Farther east, the shear zone widens and shear-zone thickness increases to about 30–60 m. In the eastern locality, no mylonite II developed within the shear zone (Fig. 3C).

Inhomogeneous deformation is emphasized by variable mylonite thickness, which is, on the regional scale, manifested by the strongly anastomosing array of the shear zones. Inhomogeneity is further demonstrated by pods of relatively undeformed wall rock that occur within the shear zones.

ANALYTICAL PROCEDURES

Mineral analyses were obtained using energy-dispersive spectrometry on a Camebax microbeam electron microprobe at Mainz University. Accelerating voltage of 15 kV, a sample current of 10 nA, and natural minerals standards were used. Peaks were obtained by iterative peak stripping and analyses were refined using a PAP program. Garnet was analyzed with a point beam (< 1 μm), whereas the beam was scanned over a 10–20 μm^2 area for feldspar, hornblende, and biotite to minimize loss of sodium and potassium. Mineral compositions were determined by averaging 3–5 analyses; the rim compositions were probed within 5 μm off the rim in garnet and within 20 μm off the rim in the other minerals. The degree of compositional zonation in the various minerals has been assessed by core and rim spot analyses. Typical analyses are presented in the Data Repository item 9912[1] and are considered to be accurate within a range of ± 3% (relative) on any given grain.

Major- and trace-element analyses were performed by standard X-ray fluorescence spectroscopy (XRF) at Mainz University, using glass-

[1]GSA Data Repository item 9912, metamorphic history of the shear zones and supplemental tables, is available on request from Documents Secretary, GSA, P.O. Box 9140, Boulder, CO 80301. E-mail: editing@geosociety.org. Web: http://www.geosociety.org/pubs/ftpyrs.htm

fusion disks and pressed-powder pellets. All analyses were made with a sequential Phillips PW 1404 wavelength-dispersive fluorescence spectrometer with excitation by an Rh X-ray tube following a method described by Stern (1972). Operating conditions were between 40 to 80 kV and 30 to 60 mA, depending on which element was analyzed.

METAMORPHIC HISTORY OF THE SHEAR ZONES

Mafwewu Hills

The wall rock displays a pronounced metamorphic banding of leucocratic and dark gray to black layers. The dark layers consist mainly of biotite, but also of large crystals of kyanite and locally garnet and hornblende. Weakly deformed rock types also contain cordierite that is altered to biotite, sillimanite, and quartz. The leucocratic bands are chiefly composed of quartz, potassium feldspar, plagioclase, and rare muscovite. Asymmetric sheared leucocratic veins are common (Fig. 4A). Details of the metamorphic history and the mineralogical changes during mylonitization for both shear zones are given in the GSA repository data (see footnote 1).

Thin extension veins occur in mylonite I and II and, more abundantly, in the wall rock (Fig. 4A). The predominant mineral in these veins is quartz. Accessory minerals, if present, generally constitute <6 vol% of a given vein in the mylonite and <3 vol% of a given vein in the wall rock. Almost no Al-bearing minerals and opaques have been observed in wall-rock veins. In mylonite, especially in mylonite II, cations were mobile and formed veins containing Mg-rich chlorite and scarce muscovite, plagioclase, biotite, sillimanite, apatite, and opaques in less-deformed pods. The Al-bearing minerals are concentrated at or near vein-rock contacts. The volume of veins is highest in the wall rock close (i.e., <5 m) to the shear-zone boundaries; typical values are between 20% and 25%, and are at most 37%. Within the mylonite, vein volume is less than 8%.

To constrain pressure-temperature (*P-T*) conditions, the garnet-hornblende thermometer (Graham and Powell, 1984) as well as the garnet + hornblende + quartz + plagioclase (GHSP) (Kohn and Spear, 1989) and the garnet + rutile + Al_2SiO_5 + ilmenite + quartz (GRAIL) (Bohlen et al., 1983) barometers have been applied. Premylonitization *P-T* conditions in the wall rock have been estimated from cores of garnet and inclusions in garnet. Temperature estimates from the garnet-hornblende thermometer yielded between 610 and 670 °C; pressure estimates range from 7.4 to 8.4 kbar (GHSP for 650 °C). Similar values have been obtained with the GRAIL

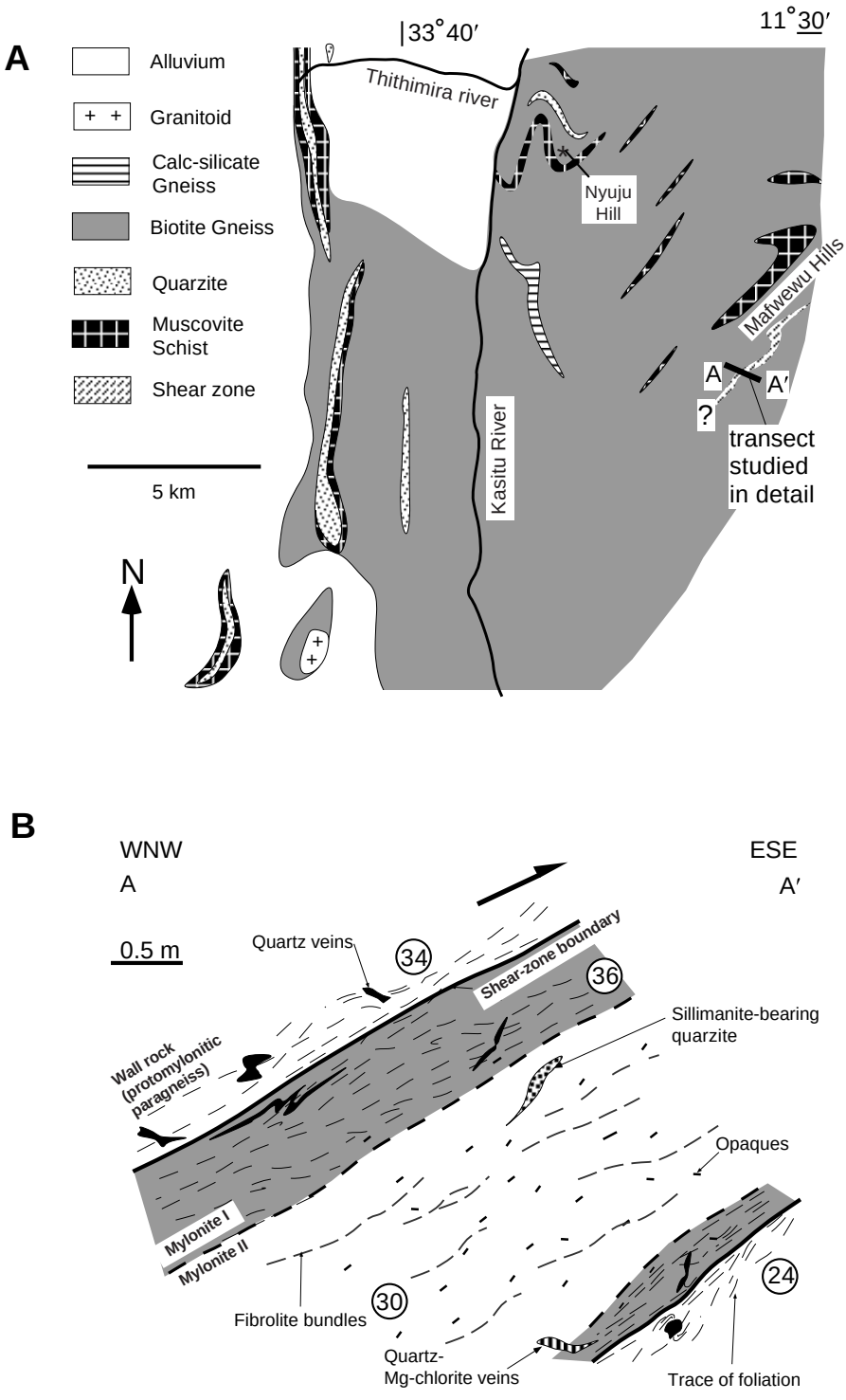

Figure 2. (A) Regional geologic map of the Mafwewu Hills shear zone (refer to Fig. 1 for location) (modified from Gaskell, 1973). Due to generally unfavorable outcrop conditions the southwestern continuation of the Mafwewu Hills shear zone is unknown. (B) Schematic sketch from the wall rock into the center of the shear zone (section is approximately perpendicular to the vorticity vector). The average mineralogies of the protolith, mylonite I, and mylonite II are given in Table 1. Circled numbers show approximate locations of some samples used in this study; all samples have the prefix Ka.

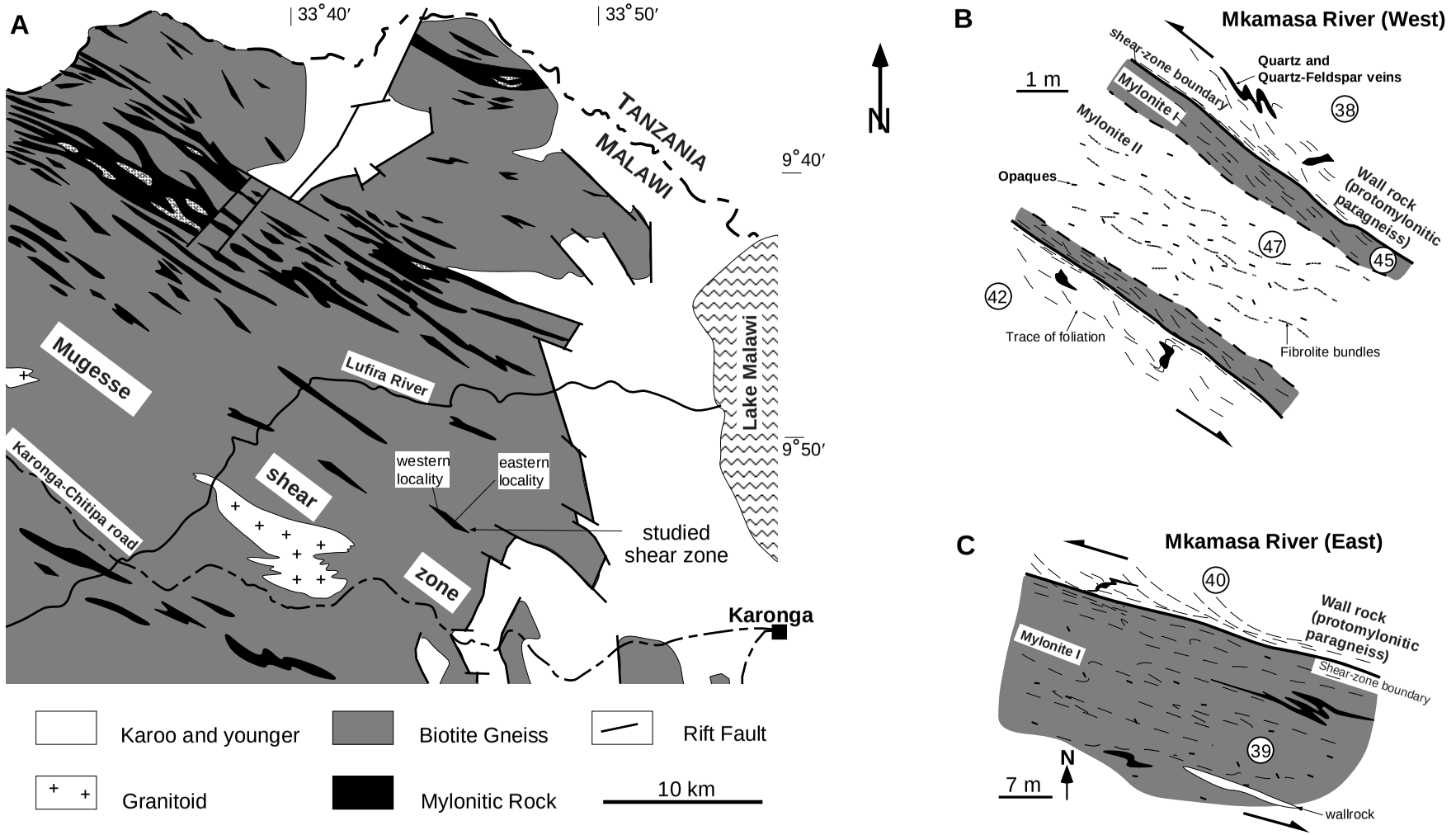

Figure 3. (A) Geologic map of the Mugesse shear zone, which developed within the Ubendian belt (for location see Fig. 1). Note the anastomosing pattern of mylonitic rocks (modified from Ray, 1975). (B and C) Schematic sketches from the protolith into the center of the shear zone for the western (B) and eastern localities (C) (sections are approximately perpendicular to the regional vorticity vector). The average mineralogies of the protolith, mylonite I, and mylonite II are given in Table 2. Circled numbers show approximate locations of some studied samples; all samples have the prefix Ka.

TABLE 1. MAFWEWU HILLS LOCALITY

Minerals	Mylonite II* (n = 3)	Mylonite I† (n = 3)	Wall rock§ (n = 6)
Quartz	41	33	32
K feldspar	4	11	11
Plagioclase	3	21	25
Garnet	7	3	3
Biotite	10	21	24
Sillimanite/kyanite	26	8	3
Opaques	9	3	2

Notes: Modal data (vol%). Al_2SiO_5 polymorph is mainly kyanite in wall rock, chiefly sillimanite in mylonite I, and exclusively sillimanite in mylonite II. Averages according to Aitchinson (1989).

*Further minerals are hornblende, zircon, sphene, apatite.

†Further minerals are hornblende, muscovite, zircon, apatite, sphene, rutile.

§Further minerals are hornblende, muscovite, chlorite, cordierite, zircon, apatite, rutile.

TABLE 2. MKAMASA RIVER LOCALITIES

Minerals	West			East	
	Mylonite II* (n = 2)	Mylonite I† (n = 3)	Wall rock§ (n = 5)	Mylonite I# (n = 4)	Wall rock** (n = 7)
Quartz	48	40	41	36	33
K feldspar	2	20	19	7	10
Plagioclase	1	16	20	18	28
Biotite	1	6	11	13	20
Muscovite	trace	1	2	2	3
Sillimanite	30	11	5	14	3
Garnet	8	2	trace	6	2
Opaques	10	4	2	4	1

Notes: Modal data (vol%). Averages calculated according to Aitchinson (1989).

*Further minerals are zircon, apatite, rutile.

†Further minerals are hornblende, zircon, sphene, apatite, rutile.

§Further minerals are hornblende, zircon, sphene, tourmaline.

#Further minerals are hornblende, zircon, sphene, apatite, rutile.

**Further minerals are hornblende, zircon, sphene.

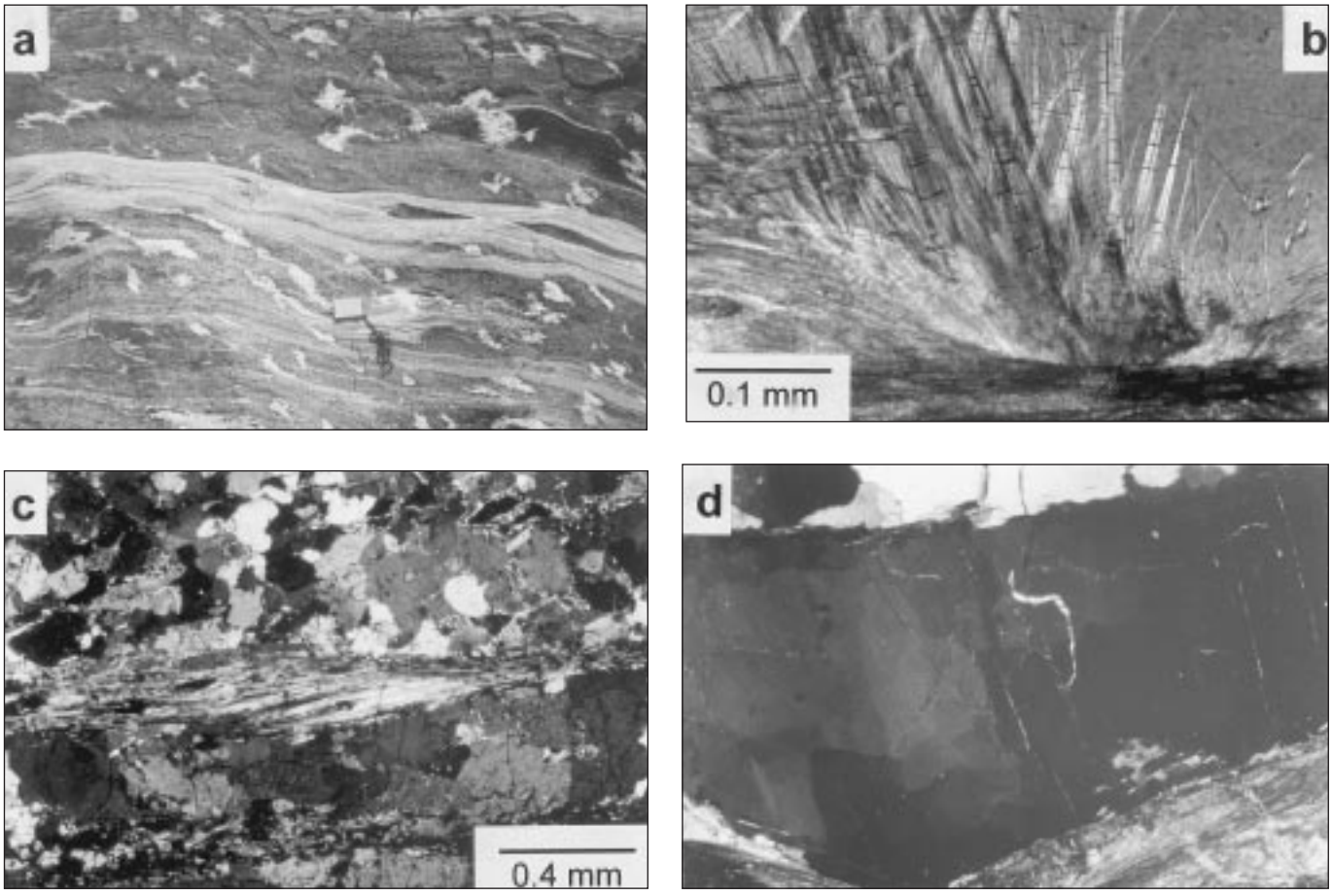

Figure 4. Photographs from Mafwewu Hills (A and C) and Mkamasa River shear zone (B and D). (A) Abundant asymmetrically sheared veins in paragneiss close to shear-zone boundary; compass in the center of the photograph gives scale. (B) Fibrolite overgrowing quartz disharmonically. (C) Development of S-C-type fabric in sillimanite bundle in mylonitic gneiss. (D) Sheared fibrolite-rich layers and large ribbon quartz. Note development of microcracks adjacent to fibrolite-rich layers. Most microcracks are stable cracks that extend from the matrix through the grain.

barometer. For *P-T* estimations in mylonite I and II, rim compositions of relict or core compositions of newly grown minerals in the mylonite have been used. The replacement of kyanite by sillimanite in mylonite I suggests a drop in pressure and/or an increase in temperature. Garnet-hornblende thermometry yielded 630–670 °C. Pressure estimates using the GHSP barometer in the mylonite supplied 6.2–6.8 kbar for a reference temperature of 660 °C. The *P-T* estimates in mylonite II yielded temperatures of 590–650 °C (garnet-hornblende thermometer) and pressures between 5.6 and 6.3 kbar (GHSP for 610 °C). The results of the thermobarometric calculations are shown in Figure 5 and are consistent with the

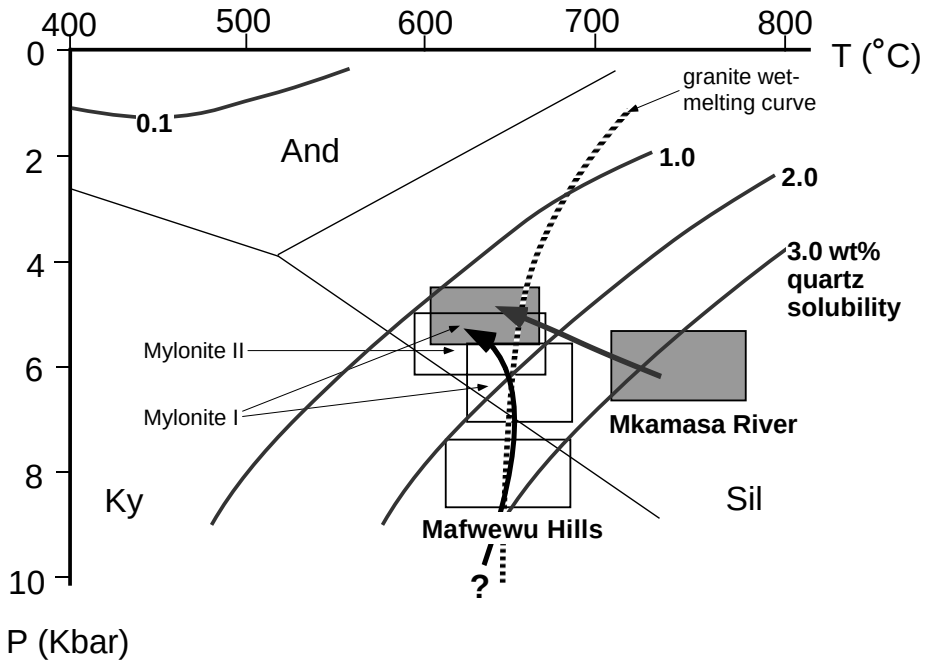

Figure 5. Inferred pressure-temperature (*P-T*) evolution for shear zones at Mafwewu Hills and Mkamasa River. Boxes indicate *P-T* conditions for various tectonometamorphic stages as discussed in text. In both shear zones, mylonitization occurred when the rocks cooled below the granite wet-melting curve. Isolines for quartz solubilities in water (in weight percent, contours labeled at the right of figure) as a function of *P* and *T* (Walter and Helgeson, 1977) are shown. Sil—sillimanite; And—andalusite; Ky—kyanite.

initiation of mylonitization during decompression. The formation of mylonite II occurs along the retrograde *P-T* path.

Mkamasa River

The paragneiss also shows a metamorphic banding into leucocratic and melanocratic layers. The dark layers consist mainly of large biotite flakes with rare sillimanite, muscovite, garnet, and hornblende. The leucocratic bands are composed of quartz, potassium feldspar, and plagioclase.

Vein minerals and vein-rock relationships for the Mkamasa River shear zone are very similar to those in the Mafwewu Hills shear zone. Accessory minerals, however, are less abundant in the Mkamasa River shear-zone veins. Where present, they generally constitute <0.5 vol% of a given vein in the wall rock and <3 vol% of a given vein in the mylonite. The volume of veins is highest in the wall rock close (i.e., <5 m) to the shear-zone boundary with typical values around 15%. Within the mylonite, vein volume is <3%.

To constrain *P-T* conditions, the GHSP barometer and the garnet-hornblende thermometer have been used. Premylonitization *P-T* conditions have been estimated from cores of garnet, plagioclase, and hornblende and the few plagioclase inclusions in garnet. Thermometry yielded between 710 and 770 °C; pressure estimates range from 5.7 to 6.7 kbar (for 725 °C). For *P-T* calculations in the mylonites, the same approach as for the Mafwewu Hills shear zone has been used. In my-

TABLE 3. MAFWEWU HILLS LOCALITY

	Mylonite II (n = 2)	Mylonite I (n = 4)	Wall rock (n = 5)
Density (g/cm^3)	2.84	2.72	2.70
SiO_2	60.67	66.32	66.10
Al_2O_3	24.41	14.11	14.15
FeO*	7.89	3.49	3.83
MnO	0.22	0.08	0.10
MgO	4.97	2.80	3.07
CaO	0.26	0.70	1.09
Na_2O	1.40	2.10	2.24
K_2O	4.96	7.20	6.60
TiO_2	1.53	0.97	0.66
P_2O_5	0.34	0.39	0.46
LOI	1.36	2.05	2.11
Total	100.01	100.21	100.35
V	123	63	64
Cr	166	136	130
Co	144	90	110
Ni	9	12	14
Zn	56	97	111
Ga	16	17	19
Rb	94	181	213
Sr	16	82	96
Y	9	24	25
Zr	342	223	181
Nb	10	4	4
Ba	171	694	710

Notes: Major elements (wt%) and minor elements (ppm). Averages have been computed according to Aitchinson (1989). LOI—loss on ignition.

TABLE 4. MKAMASA RIVER LOCALITIES

	West			East	
	Mylonite II (n = 3)	Mylonite I (n = 3)	Wall rock (n = 5)	Mylonite I (n = 4)	Wall rock (n = 5)
Density (g/cm^3)	2.89	2.65	2.61	2.73	2.68
SiO_2	62.57	71.32	71.76	64.97	69.63
Al_2O_3	27.00	14.71	13.91	17.41	13.11
FeO*	4.48	2.99	3.68	5.97	4.07
MnO	0.21	0.08	0.04	0.23	0.11
MgO	2.09	1.89	1.67	2.49	2.07
CaO	0.47	1.22	1.15	1.81	2.12
Na_2O	0.22	1.05	1.14	0.77	1.01
K_2O	0.41	3.12	3.22	3.39	4.23
TiO_2	1.47	0.95	0.92	0.84	0.71
P_2O_5	0.56	0.49	0.52	0.21	0.51
LOI	0.99	1.89	1.88	1.94	2.09
Total	100.44	99.71	99.79	100.03	99.66
V	152	63	51	87	61
Cr	244	68	57	50	33
Co	214	160	146	88	71
Ni	0	12	14	43	54
Zn	5	119	128	90	94
Ga	17	20	26	19	19
Rb	2	78	95	134	167
Sr	17	217	222	307	367
Y	9	8	8	9	11
Zr	542	299	287	184	161
Nb	15	8	7	12	9
Ba	440	340	321	204	244

Notes: Major elements (wt%) and minor elements (ppm). Averages have been computed according to Aitchinson (1989). LOI—loss on ignition.

lonite I, thermometry supplied 600–630 °C and pressure estimates are 5.3–5.7 kbar for a reference temperature of 610 °C. Due to largely unsuitable petrography, no reliable *P-T* estimates could be obtained in mylonite II. The results show that mylonitization took place as both pressure and temperature decreased (Fig. 5).

VOLUME LOSS

To investigate volume changes (Δ), major- and trace-element concentrations were plotted on isocon diagrams that compare element concentrations in the altered rock within the shear zone (C_a) to concentrations in the protolith (C_o) (Grant, 1986). The basic argument is that some components are likely to have been immobile in the alteration process and, for example, should be relatively enriched in mylonite that underwent volume loss (O'Hara and Blackburn, 1989). If these elements can be identified, they can be used to establish any volume change that has taken place. Gains or losses of other components can then be calculated assuming that the volume change is a factor common to the behavior of all components. Successful mass-balance analysis requires the geochemical reference frame be identified. The experimental results of Ayers and Watson (1991, 1993) indicate that rutile and zircon solubilities and solubility gradients in amphibolite facies *P-T* fields will be extremely low for typical water-rich fluid compositions. Ague (1994) pointed out that if significant mobility of Ti and Zr took place during metamorphism, it is likely that rutile and zircon would have grown in veins that have never been observed in and next to the studied shear zones.

The use of the isocon method implicitly assumes that an originally chemically homogeneous rock was altered. In metapelitic rocks, such an assumption is not strictly true. To overcome this problem, large samples (>5–6 kg) were collected and the results of the individual analyses averaged (Tables 3 and 4). The largest deviation between individual analyses of the major elements was about 8 wt%. Nevertheless, uncertainties arising from heterogeneous wall-rock composition and the analytical procedures (i.e., X-ray fluorescence and density estimations) limits the derivation of absolute values for volume loss and fluid/rock ratios.

Mafwewu Hills

The chemical data show that Ca, K, Na, Si, Rb, and Sr (Fig. 6), as well as P and Ba decrease systematically from wall rock to mylonite II (Table 2, Fig. 7). The decrease in the alkaline elements and Ca correlates well with the breakdown of feldspar and biotite. Ti, Fe, Al, Mg, Mn, Nb, and Zr (Fig. 6) and also Co, Cr, and V are enriched in mylonite (Table 3, Fig. 7). The relative increase in Ti, Fe, Al, Mg, and Mn can be linked to the increase in the modal abundance of sillimanite, opaques, and garnet. Although quartz increased in modal abundance, the total amount of Si in the rock decreased. A decrease in structurally bound H_2O is inferred from the decreased loss on ignition and the virtual absence of hydrous phases in mylonite II.

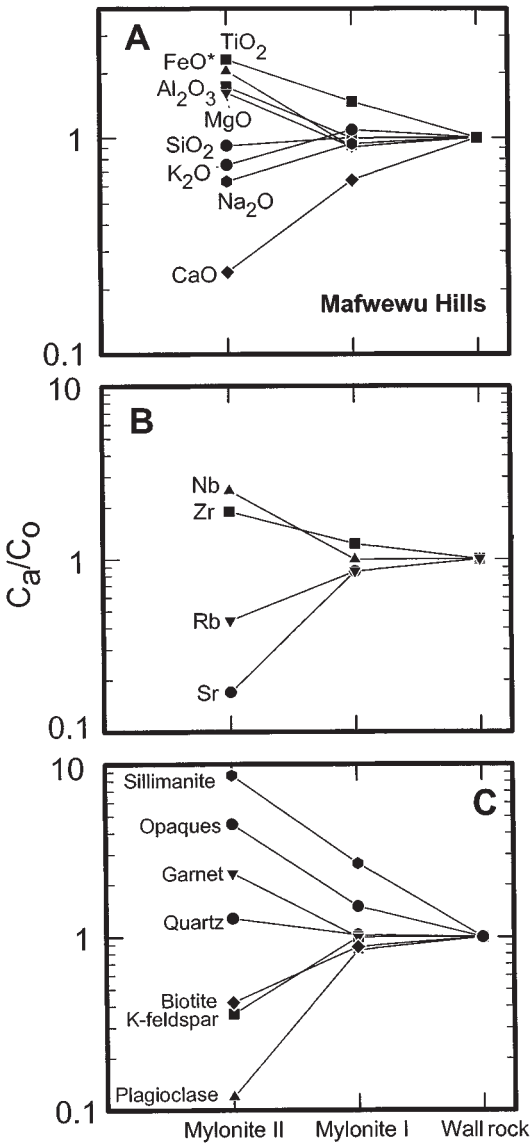

Figure 6. (A and B) Average major- and trace-element concentrations in Mafwewu Hills shear zone relative to the wall rock. C_o is the concentration of an element in the original rock, i.e., wall rock, and C_a refers to concentration in the altered rock, i.e., mylonite I or II. Note depletion in Na, K, Ca, Rb, and Sr. (C) Average change in the modal abundance of the major rock-forming minerals across the shear zone. The breakdown of feldspar and mica is in accord with element-depletion pattern in A and B. Data shown are from Tables 1 and 3. Distances on the horizontal axis are arbitrary.

The isocon diagrams in Figure 7 illustrate the depletion or augmentation of the analyzed elements during shearing. It is evident that no single isocon that suggests differential element behavior can be fitted to the data points. However, Zr and Ti plot on well-defined isocons in each of the three diagrams (Fig. 7). Elements like Al, Nb, Fe, and Mg, which are also considered to be largely immobile during amphibolite facies metamorphism (Ague, 1994), show more scatter but also depict enrichment in mylonite II. The increasing scatter of data points in the mylonite II–wall-rock plot illustrates that volume loss increases toward the center of the shear zone (Fig. 7). The development of mylonite I led to a volume loss of about 25%. The formation of mylonite II from mylonite I caused another 37% loss, resulting in an overall volume loss of 61% (referenced to wall rock) in mylonite II.

Mkamasa River

Overall, the chemical and mineralogical variation trends in the Mkamasa River shear zone are comparable to those at Mafwewu Hills (cf. Figs. 6 and 8). The variable thickness along strike of the Mkamasa River shear zone is manifested quantitatively in different mineralogical and chemical

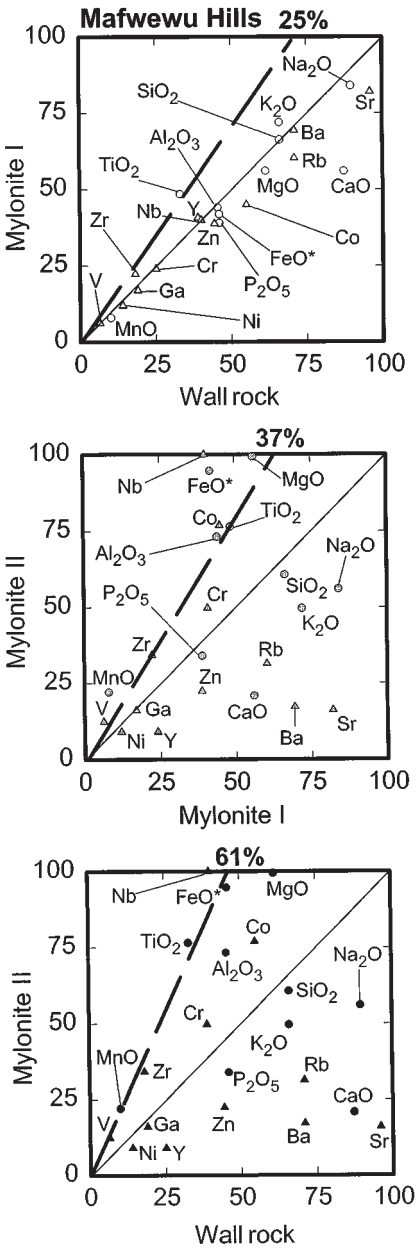

Figure 7. Isocon diagrams after Grant (1986) comparing trace-element and major-oxide concentrations in Mafwewu Hills shear zone (Table 3). Element concentrations are scaled to 0–100 wt% or parts per million. The straight line represents a 1:1 correspondence between mylonite and protolith concentrations. The mylonite has become enriched in those elements above the solid line and depleted in elements below the line. The dashed line indicates the averaged estimate of volume loss based on the enrichment of Ti and Zr. The slope of the isocon determines the volume loss according to $\Delta = (M_a/M_o)(\rho_a/\rho_o)$ (Grant, 1986). M_a/M_o is the inverse slope of the immobile Zr + Ti isocon.

changes (Tables 2 and 4), although qualitatively these trends are similar. In Figure 9, Zr and Ti again define well-constrained isocons. In the western part of the shear zone, the development of mylonite I was largely an isochemical process, whereas the switch from mylonite I to mylonite II is characterized by a considerable volume loss of 46%. In the eastern part of the shear zone, the relative enrichment in immobile elements is small, consequently the estimated volume loss in mylonite I is modest (9%).

Although there is uncertainty in these estimates, they demonstrate that shearing in both shear zones was accompanied by substantial volume loss that increased toward the center of the shear zones.

VOLUME OF FLUIDS

Assuming that the chemical changes reflect fluid-rock interaction during negative dilatation, fluid/rock weight ratios (called fluid/rock ratios herein) and the total volume of fluids infiltrating the shear zones can be estimated. Herein the scheme proposed by Newman and Mitra (1993) is used because it provides a simple framework through which a better understanding between volume loss and shear-zone thickness can be gained.

Fluid/rock ratios were estimated using silica loss and quartz-solubility data. The assumptions that underlie the calculation of the fluid/rock ratio were discussed in Newman and Mitra (1993) and generally lead to an underestimation of the fluid/rock ratio. Because the degree of quartz solubility increases drastically in the considered *P-T* range (Fig. 5) (Walter and Helgeson, 1977), fluid/rock ratios have been estimated for quartz-solubilities of 1 wt% and 2 wt%. Because there are no data on the silica concentration of the fluids circulating within the shear zone, the fluid/rock ratio has been estimated over a wide range of saturation levels (Table 5). The volume of fluid that passed through the shear zone has been estimated by multiplying the fluid/rock ratio by columns of rock with unit cross-sectional area and height equal to the thickness of the fault zone prior to deformation (Newman and Mitra, 1993). To estimate the volume of water that can be released by the retrograde dehydration reactions, the total amount of H_2O that is structurally bound in the wall rock has been determined from the chemical data of the water-bearing minerals (mainly biotite, but also hornblende and muscovite).

Mafwewu Hills

The method of Gresens (1967) permits mass-balance equations to be written that relate the chemistries of mylonite I and mylonite II to that of the wall rock. The calculations use the average compositions and densities shown in Table 3 and the volume loss as derived from the isocon diagrams in Figure 7. The following equations (referenced to 100 g of wall rock) can be written

$$\begin{aligned} &100\text{ g wall rock} - 16.0\text{ g } SiO_2 - 3.5\text{ g } Al_2O_3 \\ &- 1.2\text{ g FeO*} - 1.0\text{ g MgO} - 0.6\text{ g CaO} \\ &- 0.7\text{ g } Na_2O - 1.2\text{ g } K_2O - 0.2\text{ g } P_2O_5 \\ &= 75.8\text{ g mylonite I} + 0.1\text{ g } TiO_2 \\ &(\text{MnO remains unchanged}); \end{aligned} \quad (1)$$

and

$$\begin{aligned} &100\text{ g wall rock} - 41.2\text{ g } SiO_2 - 4.1\text{ g } Al_2O_3 \\ &- 0.6\text{ g FeO*} - 1.0\text{ g MgO} - 1.0\text{ g CaO} \\ &- 1.7\text{ g } Na_2O - 4.6\text{ g } K_2O - 0.3\text{ g } P_2O_5 \\ &= 51.0\text{ g mylonite II} \\ &(\text{MnO and } TiO_2 \text{ remain unchanged}). \end{aligned} \quad (2)$$

These equations show that the bulk of the volume loss was achieved by progressive depletion of silica toward the center of the shear zone. All other elements depict less than about 4% gain or loss relative to wall rock. Ti and Mn remain unchanged during the alteration process, whereas Al appears to be slightly mobile.

A quartz solubility of about 2 wt% appears to be reasonable for the *P-T* conditions during my-

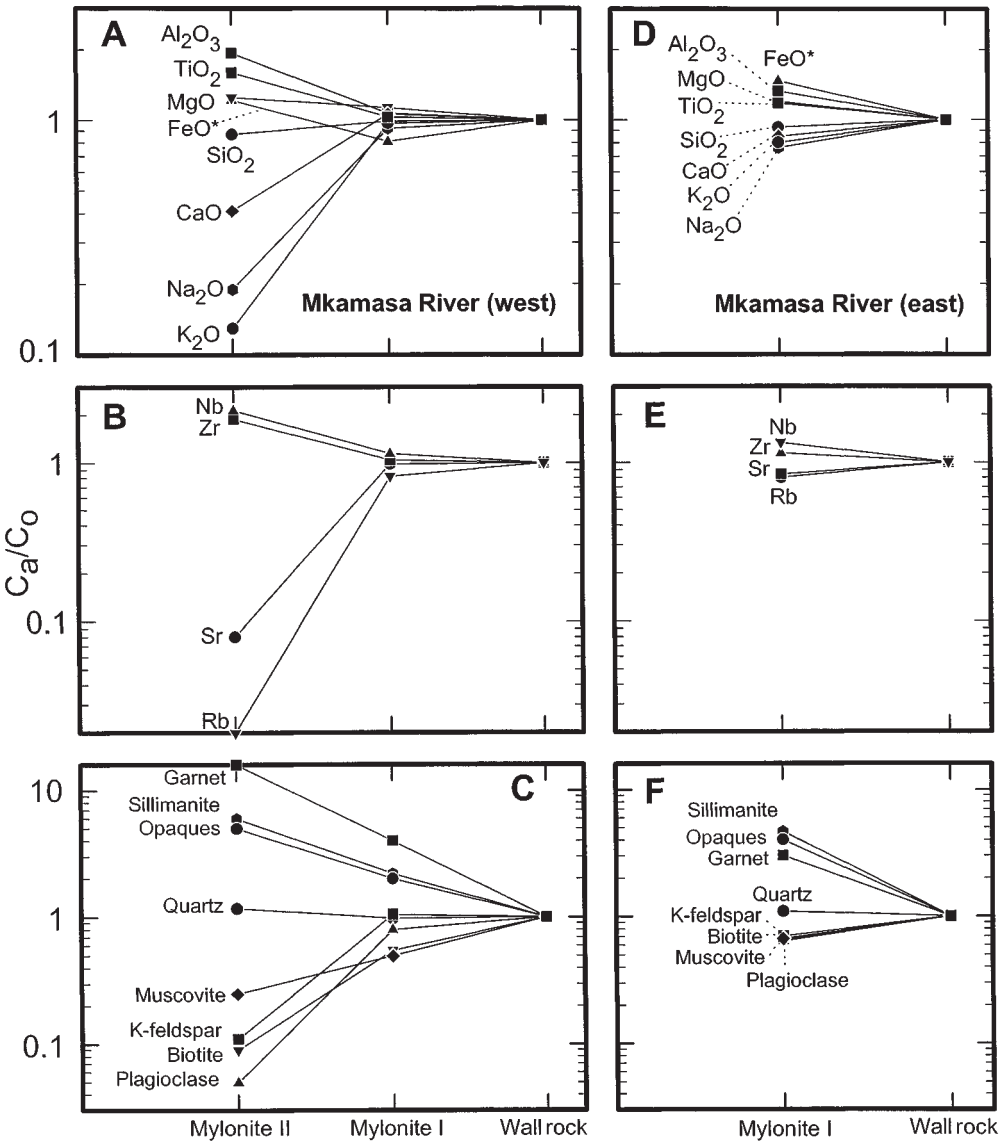

Figure 8. (A and B) Average major- and trace-element concentrations in Mkamasa River shear zone relative to wall rock. (C) Average change in the modal abundance of the major rock-forming minerals across the shear zone. The data depict the same trends as those from Mafwewu Hills (Fig. 6); note the more pronounced compositional shifts in the western part of the Mkamasa River shear zone. Data shown are from Tables 2 and 4. Distances on the horizontal axis are arbitrary.

lonitization at Mafwewu Hills. The fluids infiltrating the shear zone were probably highly saturated with respect to silica (see following discussion), hence it appears to be realistic to assume that the fluids were approximately 90% saturated with silica. Accordingly, fluid/rock ratios of ~80 for mylonite I and ~200 for mylonite II are estimated. The volumes of fluid that passed through mylonite I and II rock columns were about 100 m^3 and 1000 m^3, respectively (Table 5). The volume of structurally bound water in the wall rock is 2.8 wt%. For comparative purposes, this estimate has again been multiplied by columns of rock with unit cross-sectional area and height equal to the thickness of the entire shear zone prior to deformation. Table 6 shows that the total volume of water that could be potentially released in this column is ~0.2 m^3. The actually released volume of water is somewhat less, because water-bearing minerals still exist in the mylonite. From this exercise it can be concluded that the retrograde dehydration reactions had no influence on the fluid budget in the shear zone.

Mkamasa River

For the western part of the Mkamasa River shear zone the following mass-balance equations can be written

$$\begin{aligned} &100\text{ g wall rock} - 1.5\text{ g } SiO_2 - 0.7\text{ g FeO*} \\ &- 0.1\text{ g } Na_2O - 0.2\text{ g } K_2O \\ &= 98.4\text{ g mylonite I} + 0.6\text{ g } Al_2O_3 \\ &+ 0.2\text{ g MgO} + 0.1\text{ g CaO} \end{aligned} \quad (3)$$

(TiO_2, P_2O_5, and MnO remain unchanged).

$$\begin{aligned} &100\text{ g wall rock} - 38.6\text{ g } SiO_2 \\ &- 1.3\text{ g FeO*} - 0.6\text{ MgO} - 0.9\text{ g CaO} \\ &- 1.0\text{ g } Na_2O - 3.0\text{ g } K_2O - 0.1\text{ g } TiO_2 \\ &- 0.2\text{ g } P_2O_5 = 54.6\text{ g mylonite II} \\ &+ 0.4\text{ g } Al_2O_3 + 0.1\text{ g MnO}. \end{aligned} \quad (4)$$

Volume loss was again dominantly accomplished by progressive depletion of silica, while all other elements depict minor gains or losses. Assuming once more a 90% silica-saturated fluid and quartz solubility of 1 wt%, a fluid/rock ratio of ~400 in mylonite II is estimated. The volume of fluid that passed through the above defined column of mylonite II was on the order of 2400 m^3 (Table 5). The volume of structurally bound water in the wall rock is 1.8 wt%, which results in a total volume of water in the rock column of ~0.1 m^3 (Table 6).

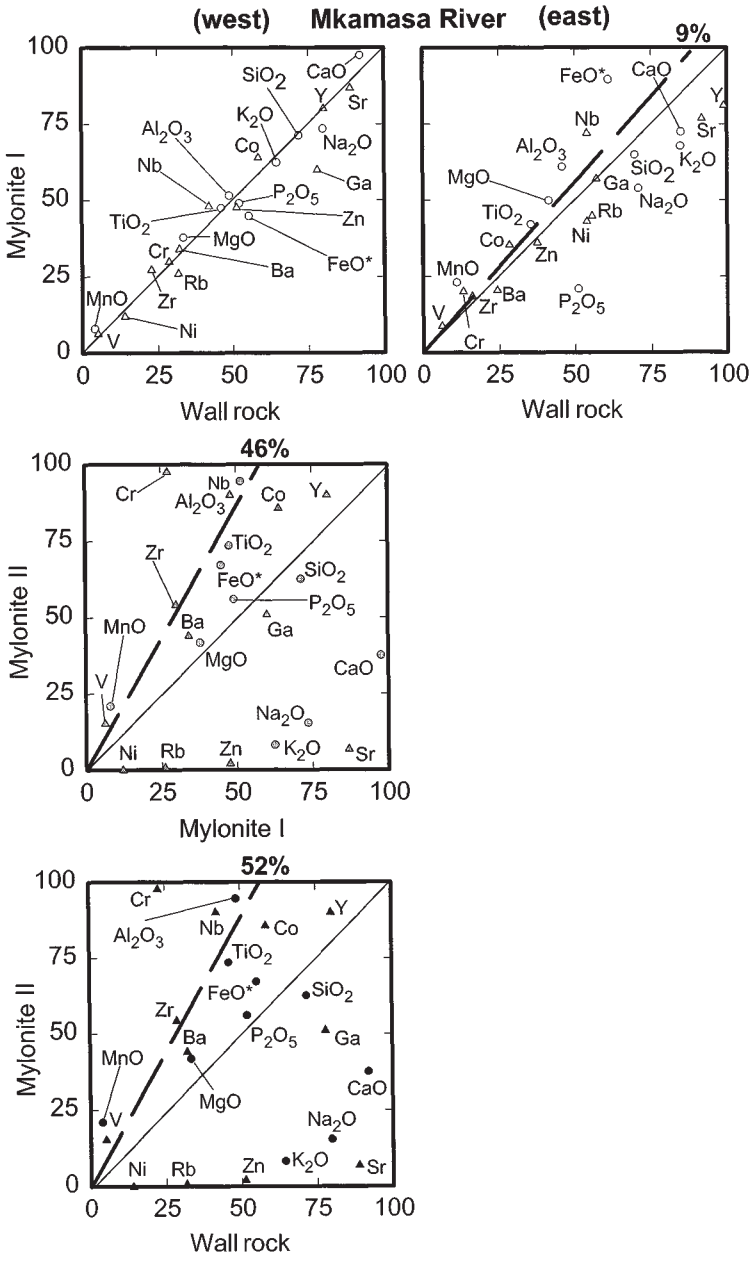

Figure 9. Isocon diagram comparing trace-element and major-oxide concentrations in Mkamasa River shear zone (Table 4). Element concentrations are scaled to 0–100 wt% or parts per million. For further explanation refer to caption of Figure 7.

For the eastern part of the Mkamasa River shear zone, I write the following equation:

$$100\text{ g wall rock} - 9.4\text{ g } SiO_2 - 0.4\text{ g CaO} - 0.3\text{ g } Na_2O - 1.1\text{ g } K_2O - 0.3\text{ g } P_2O_5 = 93.4\text{ g mylonite} + 3.0\text{ g } Al_2O_3 + 1.5\text{ g FeO*} + 0.1\text{ g MnO} + 0.2\text{ g MgO} + 0.1\text{ g } TiO_2. \quad (5)$$

The estimated fluid/rock ratio in mylonite I is ~100, and the volume of water that infiltrated the mylonite column is ~5000 m^3 (Table 5). The volume of structurally bound water in the wall rock is 2.2 wt%, creating 1.2 m^3 of water that could be potentially released within the considered rock column (Table 6).

Comparing the two outcrops in the Mkamasa River shear zone shows that the fluid/rock ratio in the center of the shear zone was about four times higher in the relatively thin mylonite zone in the west, but the volume of infiltrating fluid was only about twice as much in the more-than 10 times thicker mylonite zone in the east (Table 5). Estimating the volume of fluid for a 1 m^3 block in the center of the shear zone shows that mylonite II in the western part of the Mkamasa River shear zone was infiltrated by 800 m^3 of fluid, whereas the mylonite in the eastern part of the shear zone was infiltrated by only 100 m^3 of fluid.

DEFORMATION ANALYSIS

Prominent structures in the wall rock and within the studied shear zones are a penetrative schistosity associated with a mineral stretching lineation and mesoscale, isoclinal to tight, shear-zone–related folds. The schistosity is marked by the metamorphic banding. The foliation planes show a ubiquitously anastomosing pattern at all scales. Due to postmylonitic folding, the orientation of the schistosity may vary. The stretching lineations are either characterized by the preferred alignment of sillimanite and hornblende needles or by ductilely stretched feldspar-quartz aggregates. For a more thorough analysis of the regional deformation, see Ring (1993).

Mafwewu Hills

Foliation planes in and next to the shear zone dip moderately to the northwest (Fig. 10A). In protomylonitic wall rock and mylonite I, the mineral stretching lineations depict a pronounced maximum in the downdip direction of the associated foliation (Fig. 10B). Most of the shear bands associated with this stretching lineation have lower dips than the foliation in which they are developed, indicating a top-to-east-southeast sense of shear (Fig. 10C). Less than 20% of the observed shear bands are top-to-west-northwest displacing. Although the maximum of the stretching lineations in mylonite II still has the same orientation as that for the protomylonitic wall rock and mylonite I, the maximum is weaker (Fig. 10D). The majority of the shear bands still indicate a top-to-east-southeast shear sense; however, the ratio between top-to-east-southeast- and top-to-west-southwest–displacing shear bands drops to 2 (Fig. 10E). The orientation of the shear bands in mylonite II depicts a greater scatter than shear-band orientation in the protomylonite and mylonite I.

There are various generations of shear-zone–related, mesoscale folds developed in the mylonites. First-generation folds are reclined, isoclinal, and axial planar to the pervasive foliation. The wavelength and amplitudes of these folds range from several centimeters to a few meters. The hinge lines of first-generation folds are frequently, but not always, parallel to the mineral stretching lineation in the wall rock and mylonite I. The most common isoclinal folds are of the same size as first-generation folds and refold the latter and the penetrative foliation. A new foliation developed axial planar to these second-generation

TABLE 5. FLUID/ROCK WEIGHT RATIOS AND VOLUMES OF FLUID INFILTRATING THE SHEAR ZONES

Quartz solubility in water	1 wt%			2 wt%		
Silica saturation	0%	50%	90%	0%	50%	90%
Mafwewu Hills						
Wall rock/mylonite I						
Fluid/rock ratio	16	32	160	8	16	**80**
Volume of fluid (m^3)	21	43	213	11	21	**107**
Wall rock/mylonite II						
Fluid/rock ratio	41	82	412	21	41	**206**
Volume of fluid (m^3)	210	421	2113	108	210	**1056**
Mkamasa River (west)						
Wall rock/mylonite I						
Fluid/rock ratio	2	3	**15**	1	2	8
Volume of fluids (m^3)	2	3	**15**	1	2	8
Wall rock/mylonite II						
Fluid/rock ratio	39	77	**386**	19	39	193
Volume of fluids (m^3)	244	481	**2413**	119	244	1206
Mkamasa River (east)						
Wall rock/mylonite I						
Fluid/rock ratio	9	19	**94**	5	9	47
Volume of fluids (m^3)	495	1044	**5165**	275	495	2582

Notes: A range of values for the silica saturation of infiltrating fluids and for the quartz solubility in water have been assumed. Values for volumes of fluid are based on the volume-loss calculations and mylonite I and mylonite II thickness estimated for each outcrop. For the calculations reported, the following thickness estimations have been used: Mafwewu Hills: mylonite I = 1 m, mylonite II = 2 m; Mkamasa River (west): mylonite I = 1 m; mylonite II = 3 m; Mkamasa River (east): mylonite I = 50 m. Preferred estimates are in bold type.

folds, leading to a strong transposition foliation, which is commonly indistinguishable from the first foliation. The mineral stretching lineation may or may not be parallel to the axes of second-generation folds.

Because the majority of the analyzed folds are either immersed in mylonitic rocks or situated directly adjacent to the shear zone, I interpret their final orientation and geometry as related to shear-zone deformation.

The symmetry-based statistical method of Cowan and Brandon (1994) has been used to resolve the tectonic transport direction from the mesoscale folds. In the field, fold axes have been designated as either S or Z, corresponding to a counterclockwise or clockwise rotation, respectively, when viewed in the down-plunge direction of the fold axis. In a stereogram, the internal-rotation axes of the folds define a girdle with an attitude subparallel to the shear-zone boundary and the mylonitic foliation. From the distribution of S and Z axes, an average girdle has been constructed. Using strike and dip of this girdle as the rotation axis and the rotation angle, the S and Z axes are rotated so that the girdle pattern coincides with the stereogram horizontal. Furthermore, all internal-rotation axes have been converted to a common Z sense of asymmetry (Fig. 10F). The synoptic Z axis (SZA in Fig. 10F) is orthogonal to the slip vector (Cowan and Brandon, 1994), which has an azimuth of 111°, indicating top-to-east-southeast transport. This slip vector is subparallel to the maximum of the stretching lineations, hence the direction of the stretching lineations is regarded as the tectonic transport direction in the shear zone.

Because of the volume strains, simple-shear deformation within the shear zones can be ruled out. The development of conjugate sets of shear bands and folds (i.e., S- and Z-type folds), especially within mylonite II, points to a combination of coaxial and noncoaxial deformation. Quartz c-axis fabrics with a kinked outline (Fig. 11A) can be interpreted as representing general-shear deformation (e.g., Law et al., 1984). The gently inclined foliation outside the shear zone suggests a component of coaxial flattening that acted subperpendicular to the shear-zone walls. Grain shapes of quartz and feldspar have highly oblate grain shapes that become, especially for quartz, more pronounced in the center of the shear zone (Fig. 12, A and B). These observations qualitatively suggest that the degree of noncoaxiality, as expressed by the mean kinematic vorticity number W_m (Passchier, 1987, 1988), is lower than 1. It should be noted that $W_m = 1$ can, at least theoretically, be produced during volume-deficient, i.e., nonsimple, shearing.

To quantify the degree of noncoaxiality, the aspect ratios of feldspar in XZ sections ($X \geq Y \geq Z$, principal axes of finite-strain ellipsoid) and the angle between their long axis and the mylonitic foliation were measured. In a general shear-flow regime, particles with an aspect ratio above a critical value will rotate until they reach a stable orientation, whereas particles below this critical value will rotate without ever finding a stable orientation (Jeffery, 1922; Ghosh and Ramberg, 1976; Passchier, 1987). According to Passchier (1987), the value of this critical aspect ratio, R_c, is a function of W_m only, and is expressed by

$$W_m = R_c^2 - 1/R_c^2 + 1. \quad (6)$$

For the Mafwewu Hills shear zone, the implied R_c values in Figure 13 suggest $W_m = 0.32$ for the wall rock, $W_m = 0.76$ for mylonite I, and $W_m = 0.63$ for mylonite II (Fig. 13). The data verify substantial deviations from simple-shear deformation.

Mkamasa River

The foliation planes in and outside the shear zone dip steeply to the north-northeast and south-southwest, respectively (Fig. 14A). In the protomylonitic wall rock and in the eastern part of the shear zone, the stretching lineations depict a strong east-northeast–trending, subhorizontal maximum (Fig. 14B). Most (87%) of the shear bands associated with the protomylonitic and mylonitic stretching lineation indicate a sinistral sense of shear (Fig. 14C). In the western part of the shear zone, especially in mylonite II, the stretching lineations show a large scatter and a weak subvertical maximum (Fig. 14D) that is perpendicular to the maximum in the wall rock and in the eastern part of the shear zone. Shear-sense indicators on horizontal planes in mylonite II indicate sinistral and dextral motion (Fig. 14E). Some shear bands in Figure 14E have a shallow inclination and suggest motion out of the shear zone. The majority of the shear bands still indicate a sinistral sense of shear (21 out of 32).

Mesoscale folds, with amplitudes ranging from 10 cm to ~2 m, are developed. First-generation folds are isoclinal and the penetrative foliation is axial planar to these folds. Fold axes are variably inclined; commonly they are subhorizontal and

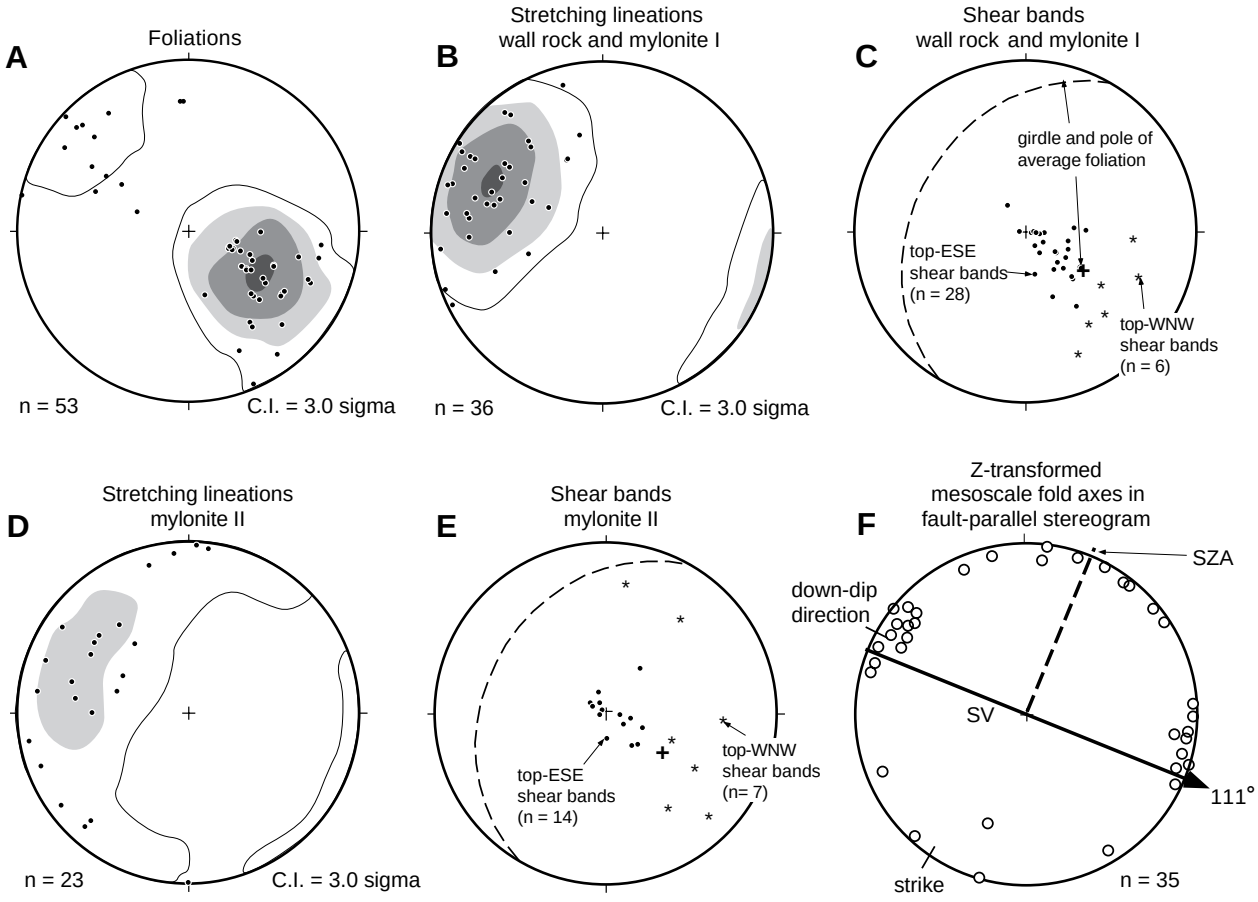

Figure 10. Orientation data for shear-zone-related structures in Mafwewu Hills shear zone, A to E in present geographic orientation. (A) Foliation planes from wall rock, mylonite I, and mylonite II. (B) Stretching lineations from protomylonitic wall rock and mylonite I. (C) Orientation of shear bands in wall rock and mylonite I. (D) Stretching lineations from mylonite II; note spread in directions, although the maximum is comparable to the maximum in B. (E) Orientation of shear bands in mylonite II; note slightly larger scatter of shear-band orientations and the increased abundance of antithetic shear bands as compared to wall rock and mylonite I. (F) Synoptic analyses of mesoscale folds using method of Cowan and Brandon (1994). Shown is a projection in which all mesoscale folds (with S and Z asymmetries) have been converted to a common Z sense of rotation (Z-transformed internal-rotation axes) and have been rotated into a shear-zone parallel reference frame. The diagram includes both upper and lower hemisphere axes plotted without distinction. SZA is the best-fit synoptic Z axis, SV is the constructed slip vector. Strike and dip of the shear zone are shown for reference. Contours in A, B, and D were determined using the method of Kamb (1959) and are reported in multiples of expected density for a uniform distribution; the lowest contour at 1× uniform density and the contour interval (C.I.) is also 1× uniform density.

TABLE 6. VOLUME OF WATER THAT COULD BE RELEASED BY COMPLETE DEHYDRATION OF ALL WATER-BEARING MINERALS IN THE WALL ROCK

Mafwewu Hills	Mkamasa River	
	West	East
0.2 m^3	0.1 m^3	1.2 m^3

Note: Calculations are based on the same thickness estimates as reported in Table 5.

parallel to subhorizontal stretching lineations in the wall rock and the eastern part of the shear zone. First-generation folds are strongly noncylindrical and are refolded together with the penetrative foliation by second-generation folds. The axes of the latter folds are in general subvertical. A new foliation developed in the hinge zones of second-generation folds, elsewhere the second foliation is parallel to the first foliation.

Folds having S asymmetries outnumber folds with Z asymmetries by far (S/Z ratio of 5.7). In a stereogram, the internal-rotation axes of the folds define a girdle that has an attitude subparallel to the shear-zone boundary and the mylonitic foliation. To illustrate the dominance of S folds, all fold axes have been converted to a common S sense of rotation and are rotated into a fault-parallel orientation (Fig. 14F). The estimated slip vector has an azimuth of 108° and is gently inclined, indicating sinistral transport. The slip vector is subparallel to the maximum of the stretching lineations in the wall rock and in the eastern part of the shear zone, hence the direction of these stretching lineations is regarded as the tectonic transport direction in the shear zone. Since this analysis of the mesoscale folds covers the entire shear zone, the stretching lineations in mylonite II in the western part of the shear zone do not reflect tectonic transport.

Conjugate sets of shear bands, the gently in-

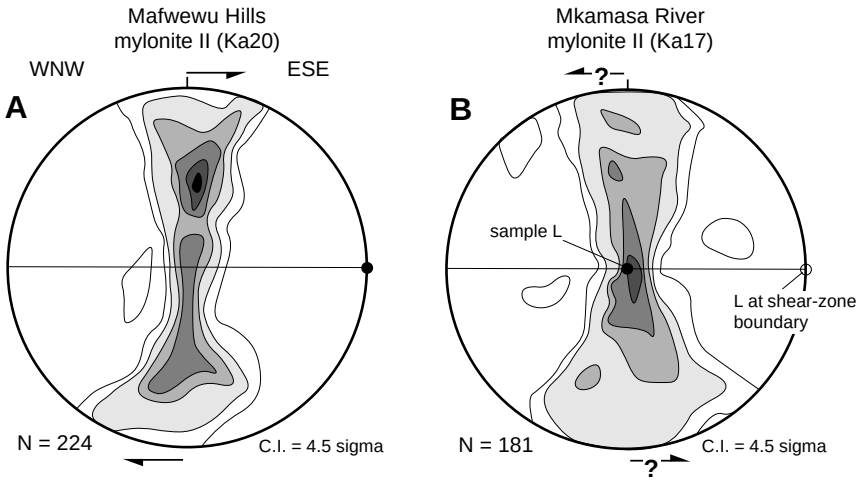

Figure 11. Quartz c-axis patterns from mylonite II from (A) Mafwewu Hills and (B) the western part of the Mkamasa River shear zone. Mylonitic foliation (straight line), stretching lineation (black dot), and deduced sense of shear (arrows) are indicated. In B, the orientation of the stretching lineation (L) at the shear-zone boundary (open dot), which reflects the regional tectonic transport direction (see text), is also shown. Both fabrics have a kinked or roughly orthorhombic topology, suggesting a high degree of coaxial deformation. Contours are according to Kamb (1959) and are reported in multiples of expected density for a uniform distribution; the lowest contour at 1.5× uniform density and the contour interval (C.I.) is also 1.5× uniform density.

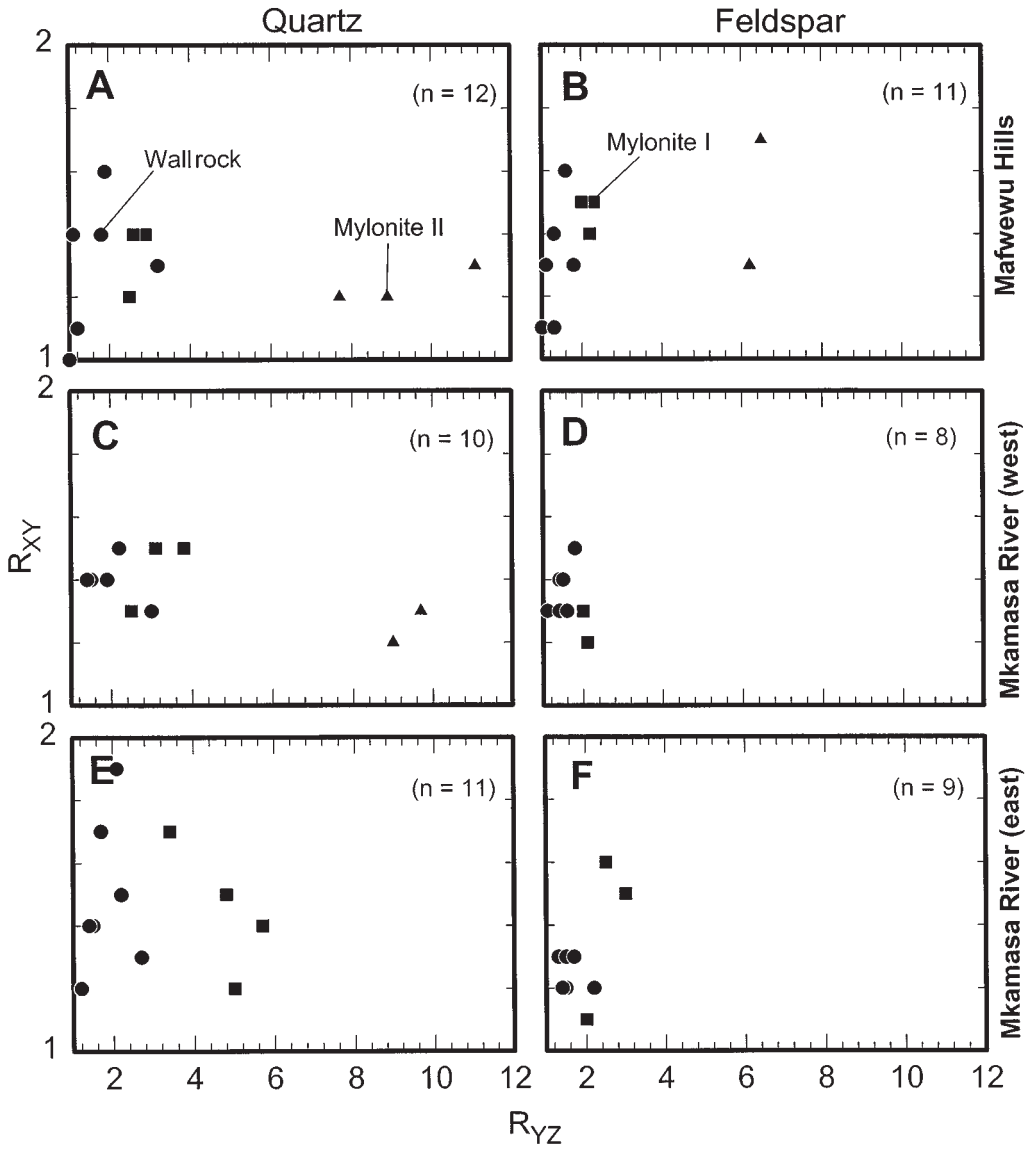

Figure 12. Aspect ratios of quartz and feldspar in foliation planes (R_{XY}) plotted against aspect ratios in planes perpendicular to foliation and lineation (R_{YZ}) (Flinn, 1962). The long and short axes of between 20 and 45 grains per section were measured and mean aspect ratios for each section were calculated. The long axes of both quartz and feldspar are oriented preferentially parallel to the foliation. The error is typically 10%–15% of the X/Y and Y/Z ratios. Note pronounced oblate geometry, especially for quartz.

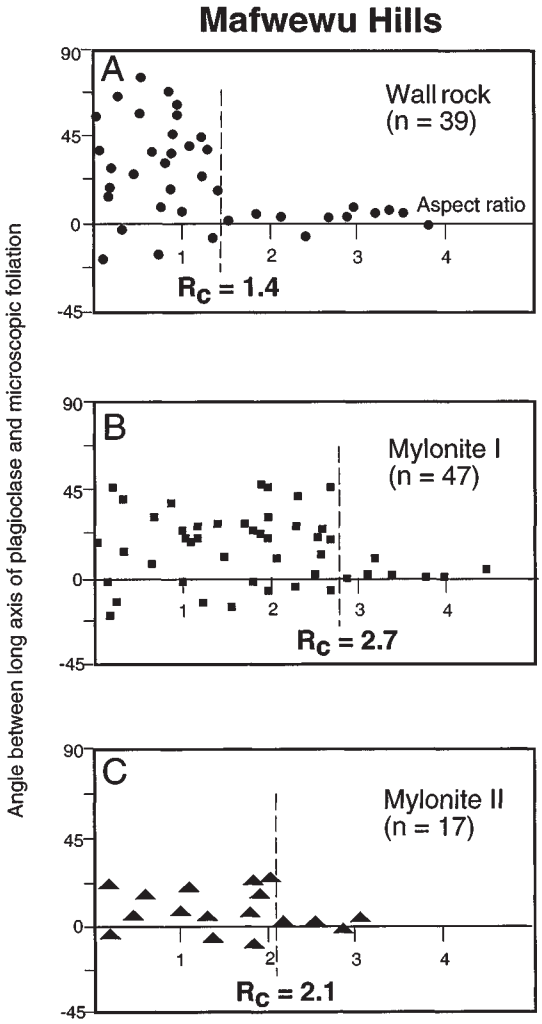

Figure 13. Porphyroblast analysis in the Mafwewu Hills shear zone. For successful flow-path analysis, the following requirements should be met (Passchier, 1987): (1) reasonably homogeneous deformation at the sample scale, (2) grain size of the matrix should be significantly smaller than the porphyroclasts, (3) finite strain should be high, (4) object shape should be regular and close to orthorhombic symmetry, and (5) sample should contain a large number of spatially well-dispersed objects. Aspect ratio values of R_c = 1.4 for the wall rock, R_c = 2.7 for the mylonite I, and R_c = 2.1 for mylonite II are inferred. Note that the R_c estimate for C is poorly defined because requirement 5 is not fulfilled; the derived W_m represents a maximum value. This analysis was done in an XZ section.

clined foliation in the wall rock with respect to the shear-zone boundary, the nearly orthorhombic topology of the quartz c-axis fabric (Fig. 11B), and the highly oblate grain shapes of quartz and feldspar grains (Fig. 12, C–F) suggest that W_m in the shear zone is lower than 1. The quantification of W_m yields the same results as for the Mafwewu Hills shear zone and confirms strong deviations from simple shear. In the eastern part of the Mkamasa River shear zone, R_c values indicate W_m = 0.44 for the wall rock and W_m = 0.79 for mylonite I (Fig. 15). In the west, values of W_m = 0.26 for the wall rock, W_m = 0.70 for mylonite I, and W_m = 0.57 for mylonite II have been obtained.

RELATION BETWEEN DEFORMATION AND METAMORPHISM

Deformation and metamorphism relationships and their progressive change with increasing deformation are very similar in both studied shear zones. The development of the schistosity in the wall rock is expressed by a flattening of feldspar and the preferred alignment of biotite parallel to the flattened planes of feldspar. Radiating aggregates of fibrolitic sillimanite (Fig. 4B) overgrew feldspar-biotite boundaries at the margin of the shear zones. The grain boundaries of biotite and feldspar meet the prismatic faces of fibrolite at random angles, suggesting that the fibrolitic sillimanite grew disharmoniously, that is, after the final positioning of the boundaries between the other minerals (cf. Vernon and Flood, 1977).

In mylonite, biotite and feldspar are partly replaced by fibrolitic sillimanite. The long axes of both minerals are subparallel to each other. Sillimanite occasionally defines S-C-type structures (Fig. 4C). Feldspar between the biotite-sillimanite layers recrystallized synkinematically to form core-and-mantle structures. Potassium feldspar developed myrmekite structures where crystal faces are parallel to foliation planes.

With increasing deformation the amount of fibrolite, garnet, and opaques, and to a lesser degree quartz, increased (Figs. 6 and 8). Bunches of fibrolite partly enclose relics of biotite. Between fibrolite layers, ribbon quartz with aspect ratios of as much as 14 developed. The grain boundaries of quartz meet the fibrolite bundles approximately at 90° angles, suggesting that fibrolitic sillimanite grew harmoniously (cf. Vernon and Flood, 1977) before or during the development of the quartz ribbons. Quartz between fibrolite bundles commonly shows microcracks (Fig. 4C) that formed at a high angle to the fibrolite bundles. The material in the cracks appears to be fibrolite and phyllosilicate.

To explore the relationship between water-releasing biotite breakdown and the related enrichment of sillimanite + quartz and deformation, the sillimanite/biotite ratio has been plotted against the aspect ratio of quartz in XZ sections and against the number of microcracks in quartz (Fig. 16). Both sets of diagrams show virtually the same trend: (1) a pronounced increase in strain (as represented by the aspect ratios of quartz and the number of microcracks in quartz) at very low sillimanite/biotite ratios (~<0.3), and (2) the increase in strain slows down, but gets very high as biotite is intensively replaced by sillimanite. These trends are especially conspicuous in mylonite II.

The notable increase in strain at low sillimanite/biotite ratios is probably solely due to deformation, because the sillimanite-producing reaction had not yet proceeded significantly. Deformation at this stage is characterized by sliding and local boudinage of biotite along (001) planes and the formation of deformation lamellae, strong undulose extinction, and subgrain structures in quartz. These processes tend to increase the total surface area of biotite and quartz, leading to high internal free energy (Vernon, 1976; Passchier and Trouw, 1996), which in turn triggers mineral reactions or en-

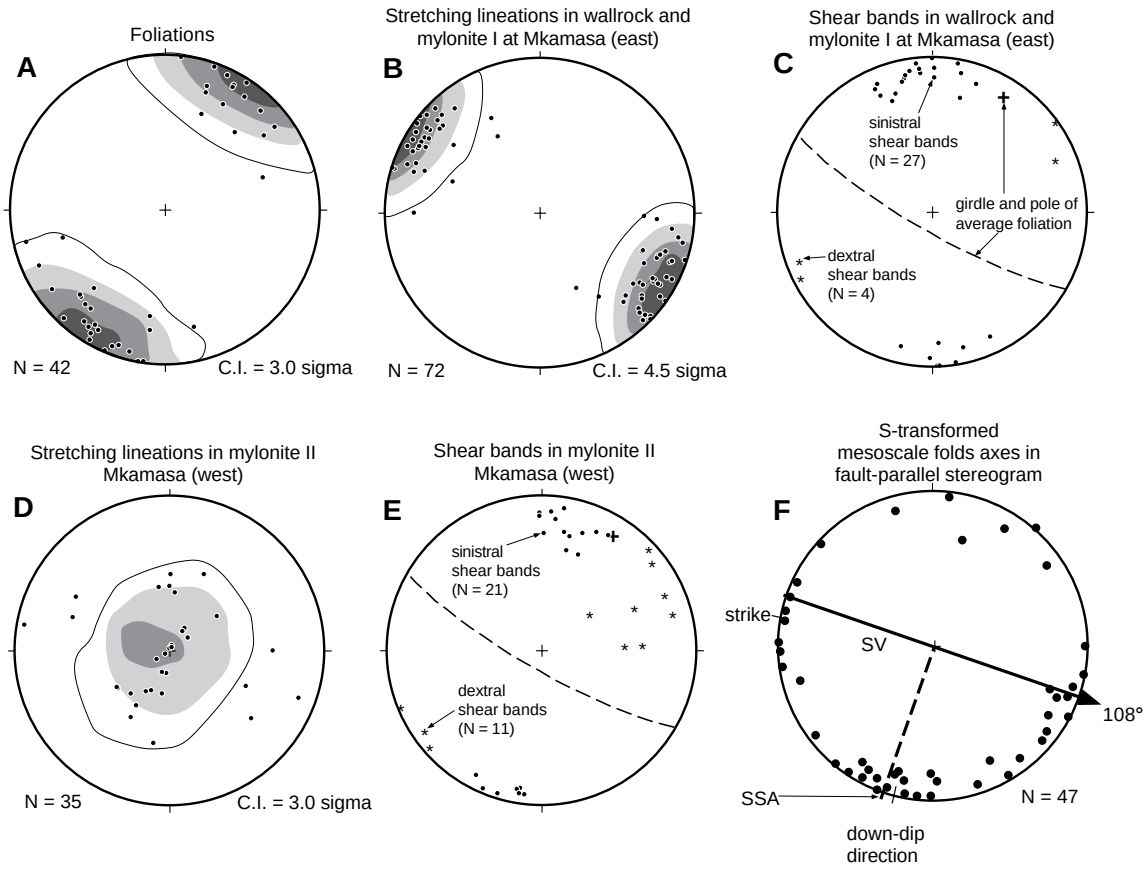

Figure 14. Orientation data for shear-zone–related structures in Mkamasa River shear zone; (A–E) in present geographic orientation. (A) Foliation planes from wall rock, mylonite I, and mylonite II from eastern and western parts of the shear zone. (B) Stretching lineations from protomylonitic wall rock and mylonite I from eastern part of the shear zone; note very strong maximum (the contour parameters are different in this stereogram, see following). (C) Orientation of shear bands in wall rock and mylonite I (eastern part of shear zone). (D) Stretching lineations from mylonite II in western part of the shear zone; note spread in directions and subvertical maximum perpendicular to maximum in the protomylonitic wall rock and mylonite I. Contours as in Figure 10, except for B, where the lowest contour and contour intervals (C.I.) are at 1.5× uniform density. (E) Orientation of shear bands in mylonite I (western part of shear zone); note slightly larger scatter of shear-band orientations and the increased abundance of antithetic shear bands as compared to the wall rock and mylonite I from the eastern part of the shear zone. (F) Synoptic analyses of mesoscale folds from the entire shear zone in fault-parallel reference frame. Note that all folds have been converted to common S sense of rotation, hence all vectors have a "left-handed" sense of rotation according to the convention of Means et al. (1980). The strike of the shear zone is subparallel to SV, indicating a very low inclination of SV. For further details see explanation to Figure 10.

hances rates of mineral reactions (Murrel, 1985; Wintsch, 1985); therefore, these processes may have ultimately caused the pronounced increase in the sillimanite/biotite ratio.

The number of microcracks shows a positive correlation with the sillimanite/biotite ratio (Fig. 16B). Flöttmann (1988) showed that the development of such microcracks in amphibolite facies rocks is due to a reduction in mean stress as a consequence of increased fluid pressure (Etheridge, 1983). The distinct spatial relationship between the microcracks, the fibrolite bundles, and the sillimanite/biotite ratio suggest that biotite breakdown to sillimanite and quartz caused an increased fluid pressure at the reaction sites.

VOLUME LOSS AND COAXIAL VS. NONCOAXIAL DEFORMATION

Figure 17A depicts that volume loss correlates positively with distortional strain (as expressed by R_{XZ} of quartz and feldspar), i.e., the more distortion that occurs, the more volume is lost. The correlation between W_m and the degree of flattening and volume loss, respectively, is less straightforward (Fig. 17, B and C). For samples with no or little volume loss (i.e., wall rock and mylonite I), a correlation between W_m and volume strain and distortion exists. Only when volume loss becomes pronounced, do the parameters not correlate anymore.

In both studied shear zones, W_m increases from the wall rock toward mylonite I, then drops to values of <~0.6 in mylonite II. The pronounced distortion of quartz and feldspar in mylonite II might thus be mainly achieved by coaxial flattening. The high R_{XZ} recorded in the distinctly volume-deficient mylonite II may in fact indicate that uniaxial volume loss was accompanied by strong contraction in Z, which was by far not balanced by extension in X and possibly Y. The high distortional strain in mylonite II would then basically be the result of pronounced contraction in Z (see also O'Hara, 1990).

The geochemical and structural data suggest that there was strain partitioning in the shear

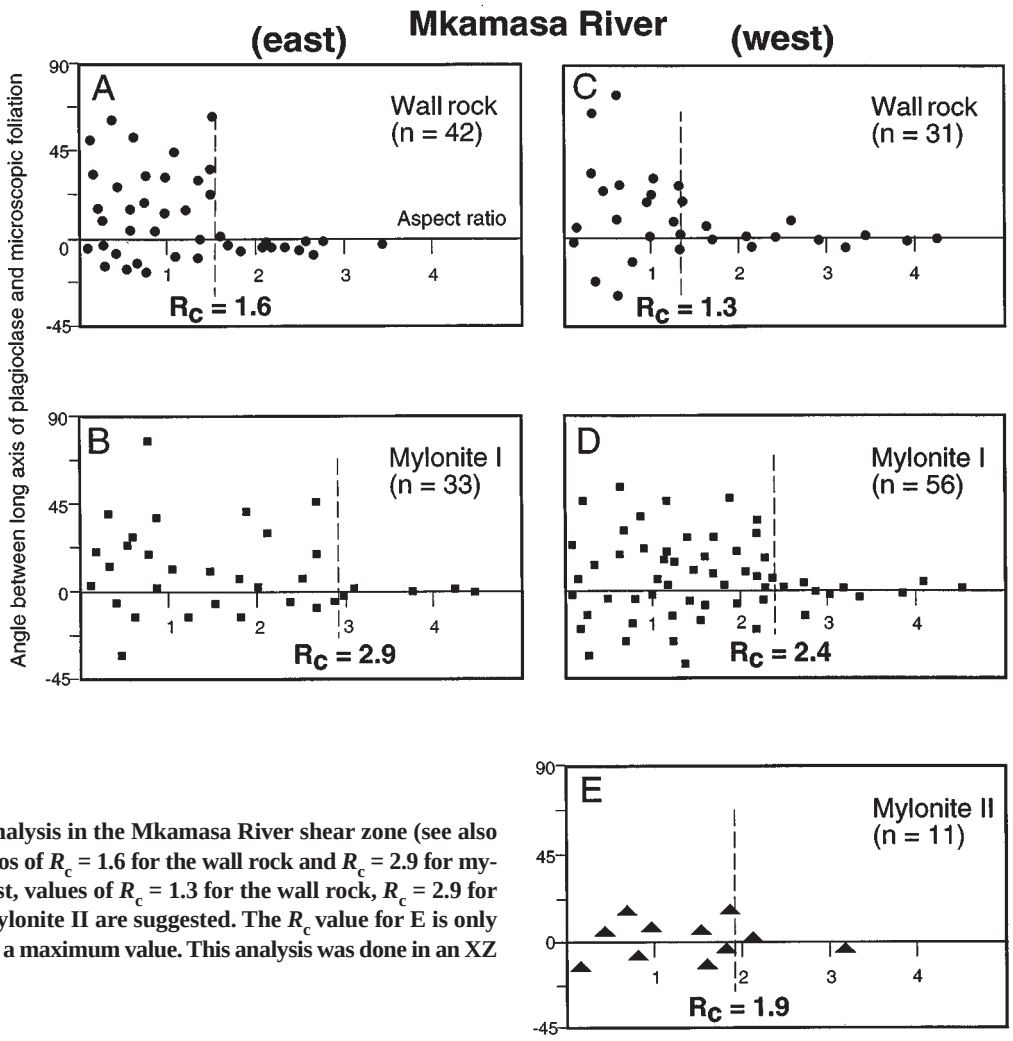

Figure 15. Porphyroblast analysis in the Mkamasa River shear zone (see also Fig. 13). In the east, aspect ratios of R_c = 1.6 for the wall rock and R_c = 2.9 for mylonite I are implied. In the west, values of R_c = 1.3 for the wall rock, R_c = 2.9 for mylonite I, and R_c = 1.9 for mylonite II are suggested. The R_c value for E is only weakly defined; W_m represents a maximum value. This analysis was done in an XZ section.

zones. Mylonite I took up most of the rotational component of deformation, whereas mylonite II is characterized by high distortional and volume strains.

DISCUSSION

Fluid Sources

Evidence has been given that the infiltrating fluid was not generated in situ. Selverstone et al. (1991), in a study of an amphibolite facies shear zone in the Tauern window of the Eastern Alps, came to a similar conclusion. These authors conceived that the infiltrating fluid originated from dehydration of flysch sequences that were underthrusted at the time the shear zone operated at a higher crustal level. Ring and Toulkeridis (unpublished data) showed that the pattern of contractional and transcurrently displacing amphibolite facies shear zones in northern Malawi occurred during a subduction and/or collision event, i.e., in a scenario in which material in the lower plate may still undergo prograde metamorphic reactions, whereas rocks in the upper plate undergo decompression and retrograde metamorphism. Dehydration reactions during prograde metamorphism create large volumes of fluid. As shown by Ague (1994), prograde metamorphism may cause volume loss of about 30% in amphibolite facies rocks. The most obvious chemical change during such volume loss is the progressive removal of silica with increasing metamorphic grade (Ague, 1994). This suggests that the liberated fluids were highly saturated with silica.

The problem with deriving fluids from deeper crustal levels is that those upward-migrating (i.e., down regional *T* and *P* gradients) fluids are not likely to dissolve large amounts of silica. In a contractional setting, however, thrusts usually place higher isotherms over lower ones and therefore create inverted thermal gradients (e.g., England and Thompson, 1984; Kohn et al., 1992; England and Molnar, 1993), thus permitting silica to be dissolved by the fluid upon passage through the shear zone. The addition of possible shear heating would increase this effect.

Most of the fluid liberated in the lower crust may have been initially consumed by melting processes. In this respect it is interesting to note that the studied shear zones formed when the rock cooled below the wet granite solidus (Fig. 5), i.e., at a time when H_2O-rich fluids became increasingly available (Bucher and Frey, 1994). In a study of an upper amphibolite facies (700–750 °C and 5–7 kbar) sinistral shear zone in the Mugesse shear zone, Ring (1997) discovered isochemical behavior of major and trace elements. A possible reason for this different behavior of shear zones that developed during the same tectonic episode but under different *P-T* conditions may be the infiltration of a solvent fluid into the shear zone,

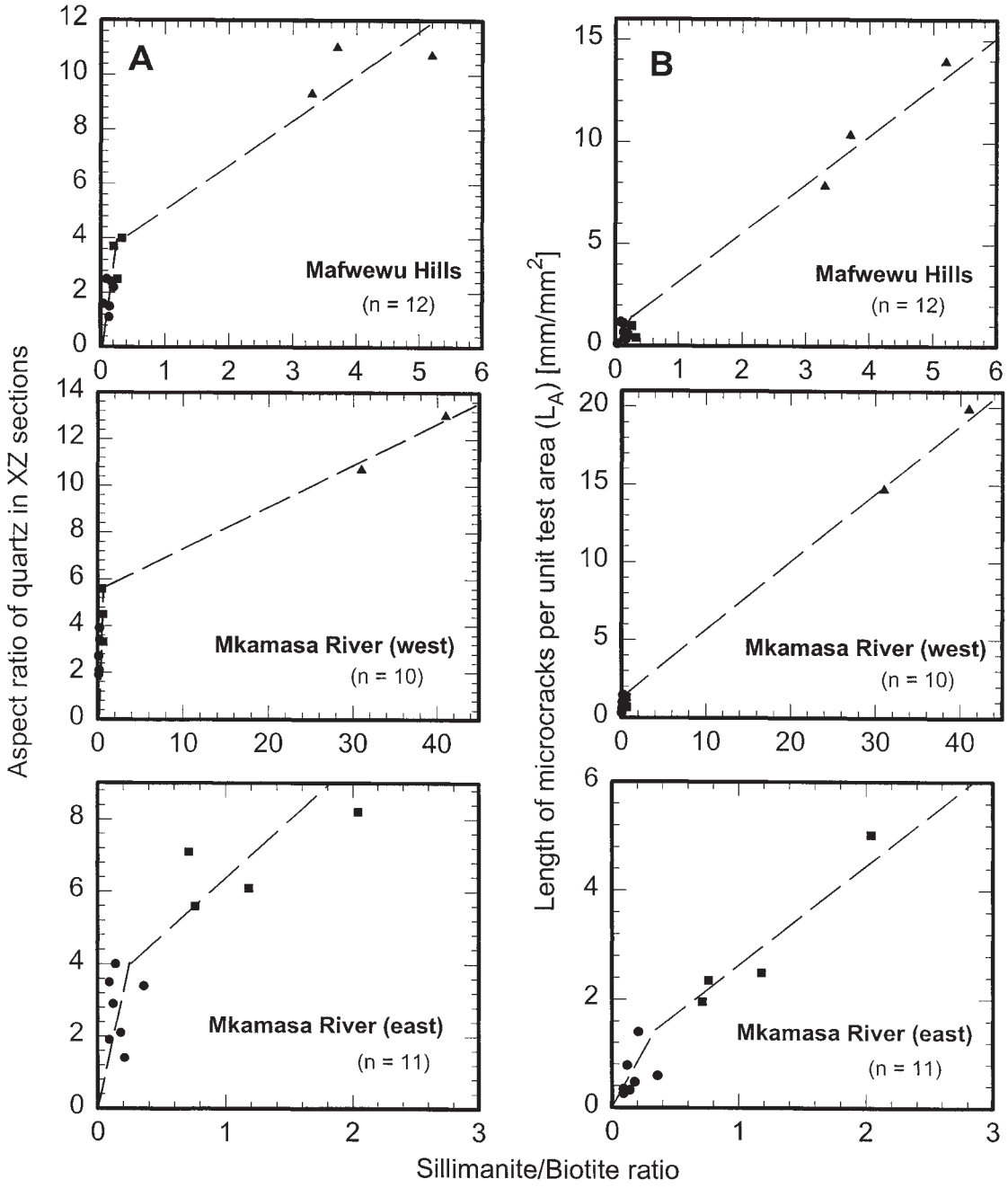

Figure 16. (A) Aspect ratio of quartz ribbons in XZ sections (R_{XZ}) plotted against the sillimanite/biotite ratio. (B) Length of microcracks per unit test area (L_A, see Underwood [1970] for details of measurements) plotted against the sillimanite/biotite ratio. Below a sillimanite to biotite ratio of ~2, microcracks do not appear to be important. Symbols for wall rock and mylonite I and II as in Figure 12.

which is more likely at temperatures below the wet granite solidus.

Retrogressive Shearing and Fluid Flow

The initiation of the shear zones is intimately associated with the growth of fibrolite and quartz from biotite and feldspar. The formation of fibrolite and quartz in high-strain zones appears to be a consequence of dehydration reactions (Vernon and Flood, 1977) and dealkalization accompanying mylonitization (Zwart, 1965), both of which caused the breakdown of biotite. Although the total amount of water liberated by this dehydration reaction is negligible with respect to the total volume of fluid that infiltrated the shear zone, the relationship between the sillimanite/biotite ratio and strain suggests that the released water had a catalytic influence on the local deformation behavior of quartz. The dealkalization within the shear zone caused the destabilization of micas and prevented the growth of new micas in the shear zone. The end product of progressive shearing is almost dry, sheet silicate–free mylonite II. Etheridge (1983) showed that the weak bonding between (001) planes in layer silicates results in higher porosity than in strongly bonded frame-

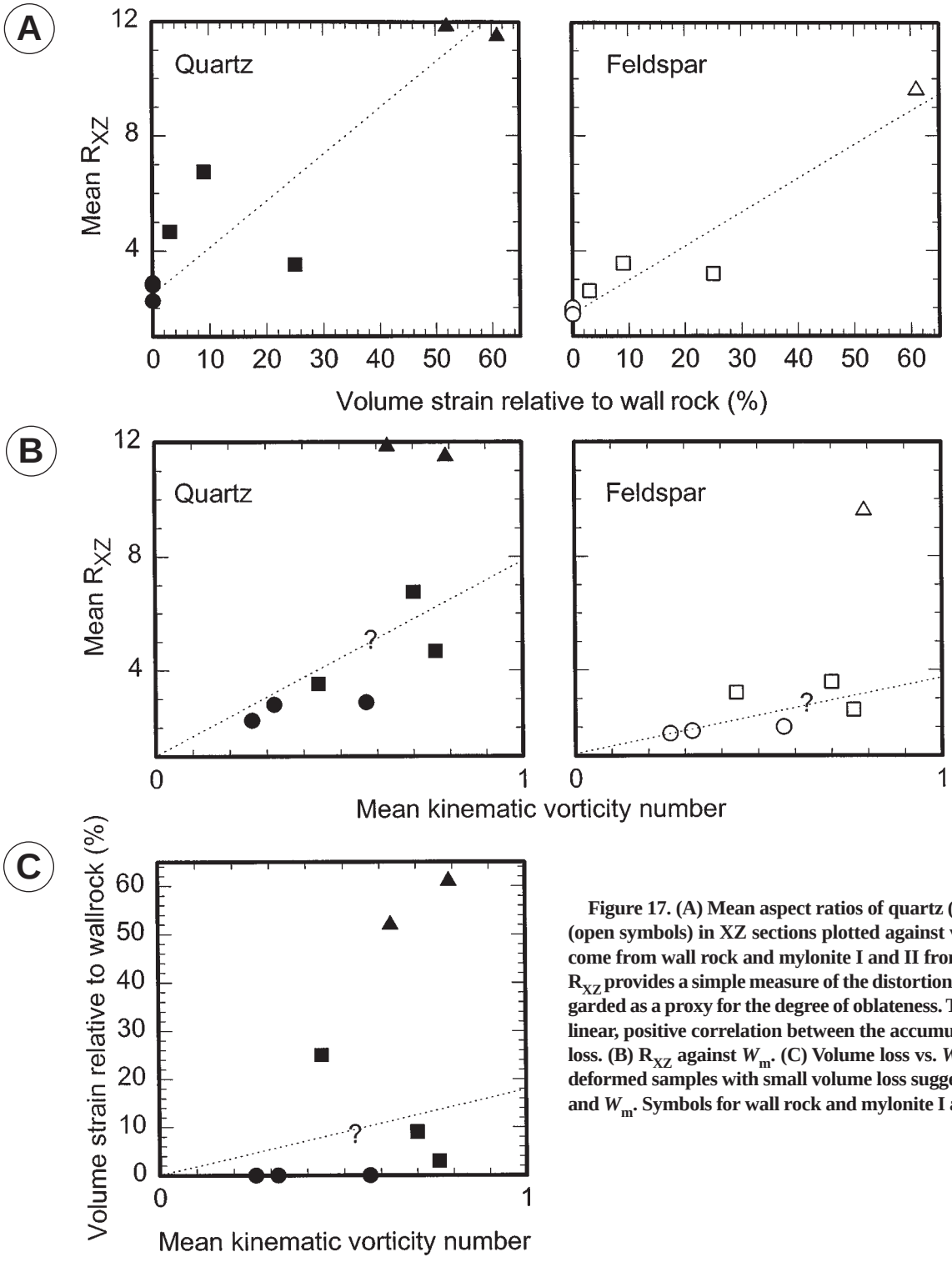

Figure 17. (A) Mean aspect ratios of quartz (bold symbols) and feldspar (open symbols) in XZ sections plotted against volume strain. The samples come from wall rock and mylonite I and II from both studied shear zones. R_{XZ} provides a simple measure of the distortional strain and can thus be regarded as a proxy for the degree of oblateness. The graphs depict an almost linear, positive correlation between the accumulation of strain and volume loss. (B) R_{XZ} against W_m. (C) Volume loss vs. W_m. In B and C, moderately deformed samples with small volume loss suggest correlation between R_{XZ} and W_m. Symbols for wall rock and mylonite I and II as in Figure 12.

work and orthosilicates. The almost complete breakdown of biotite destroyed the pathways for fluid circulation in the mylonite, which ultimately resulted in strain hardening and the cessation of shearing.

The presence of highly altered mylonite between nonaltered wall rock and the occurrence of relatively undeformed, nonaltered wall rock within the shear zones suggests that fluid flow was channelized within the shear zone. Such a view is corroborated by the large fluid/rock ratios and by the high volume loss that created porosities and thus pathways for fluids in the mylonite. The relatively large number of quartz veins directly outside the shear zones suggests that the fluid was not confined to the shear zone but also penetrated the wall rock, where dissolved material was partly precipitated. The modal abundance of veins adjacent to the shear zone, however, is too small to account for the entire volume loss in the shear zone.

Lateral Variations in the Mkamasa River Shear Zone

A remarkable feature of the Mkamasa River shear zone is the lateral variation of its overall structure. The large volume loss, high fluid/rock ratio, and stretching lineations oriented subperpendicular to the shear direction in the thin (~4 m) mylonite zone in the west compare to relatively little volume loss, a lower fluid/rock ratio, and a normal, i.e., transport-parallel, orientation of the stretching lineations in the thick (~50 m) mylonite zone in the east. Newman and Mitra (1993) reported a similar variation in fault-zone structure from the Linville Falls fault zone in the southern Appalachians and attributed it to differences in feldspar composition in the wall rock.

In the western part of the Mkamasa River shear zone, wall rock and mylonite I consist of relatively little biotite (11% and 6%, respectively) as compared to the shear zone in the east (20% and 13% biotite). The amount of framework and orthosilicates in the west increases toward the center of the shear zone (75% → 79% → 89%), whereas in the east the amount of framework and orthosilicates is reduced in mylonite I (76% → 71%). As discussed herein, the weak bonding between (001) planes in layer silicates results in higher porosity than in strongly bonded framework and orthosilicates. Accordingly, the relatively large amount of biotite relative to framework and orthosilicates helped fluids infiltrate a larger volume of rock in the east. In the western part of the Mkamasa River shear zone, the infiltration of fluid was more difficult, hence a relatively thin zone with a high fluid/rock ratio developed. This high fluid/rock ratio aided diffusion processes at grain boundaries and may have caused dissolution and transport of silica, causing the large volume loss in the west.

Newman and Mitra (1993) compared variations in fluid flow along the Linville Falls fault zone to the grain-boundary model of islands and channels (Mott, 1948; Raj and Chyung, 1981). Channels are represented by thin zones having high fluid/rock ratios and islands are characterized by thick zones having low fluid/rock ratios (Newman and Mitra, 1993). The structural data indicate that the degree of coaxial deformation was higher in the thin western part (i.e., channel) of the Mkamasa River shear zone than in the broad eastern part (i.e., island). According to the earlier discussion herein, the formation of the channels may have been aided by an increased amount of shear-zone–perpendicular contraction. On a larger scale, such a fluid-flow and strain partitioning ultimately results in an anastomosing pattern of shear zones. The Mugesse shear zone of northern Malawi (Fig. 3A) may reflect a regional-scale island and channel structure.

The transport-normal orientation of the stretching lineations in the western part of the Mkamasa River shear zone indicates that the maximum principal elongation became the axis of the rotational component of deformation. This orientation of the stretching lineations was controlled by the pure-shear component of deformation because fabric elements can rotate faster in pure shear than in simple shear (Pfiffner and Ramsay, 1982). Robin and Cruden (1994) argued that in transpressional zones the vorticity vector is commonly not parallel to any of the principal directions of strain and the deformation has a triclinic symmetry. Such a case has not been observed in the Mugesse shear zone, where stretching lineations tend to be either subparallel or subperpendicular to tectonic transport. Passchier (1987) demonstrated that material lines tend to reach stable positions, i.e., rotate toward an axis that coincides with the extending irrotational material line of deformation (called "fabric attractor" by Passchier, 1997). Therefore, a triclinic deformation geometry does not appear to be a favorable symmetry in deforming zones.

CONCLUSIONS

The following conclusions can be drawn from this study.

1. The two studied retrograde shear zones in the Proterozoic crust of northern Malawi are characterized by the progressive breakdown of feldspar and biotite to form sillimanite, quartz and water. The shear zones developed under amphibolite facies *P-T* conditions below the wet granite solidus and are characterized by high fluid/rock ratios and considerably negative volume strains.

2. The bulk of the volume loss was achieved by loss of silica. A dramatic consequence of the high fluid flow was an almost complete dealkalization within the shear zone. The associated destabilization of micas destroyed the pathways for fluid circulation, dried out the shear zone, and ultimately caused the cessation of shearing.

3. Strain geometry within the shear zones is oblate. The distortional strain correlates positively with volume strain. Mean kinematic vorticity numbers demonstrate a substantial component of coaxial deformation. All this indicates that deformation in the studied shear zones did not accumulate by progressive simple shear.

4. In parts of the transcurrently displacing Mkamasa River shear zone that are characterized by the largest amounts of volume loss (~60%) and small kinematic vorticity numbers, shear-zone–related stretching lineations developed perpendicular to tectonic transport. This indicates that the maximum principal elongation is the axis of the rotational component of deformation. In this case, the pure-shear component of deformation is controlling the final orientation of the stretching lineations.

ACKNOWLEDGMENTS

This study is part of the Hominid Corridor Research Project (HCRP), which has been funded by the Deutsche Forschungsgmeinschaft and National Geographic Society. HCRP is conducted by authority of the Department of Antiquities and the Ministry of Culture and Education of Malawi under the auspices of Yusuf Juwayewi, whom I thank. A presubmission review by Thomas Flöttmann, formal reviews by Kieran O'Hara and Gautam Mitra, and editorial assistance by Douglas Walker and John Geissman helped to clarify the ideas presented in the paper.

REFERENCES CITED

Ague, J. J., 1994, Mass transfer during Barrovian metamorphism of pelites, south-central Connecticut. I: Evidence for changes in composition and volume: American Journal of Science, v. 294, p. 989–1057.

Aitchinson, J., 1989, Measures of location of compositional data: Mathematical Geology, v. 21, p. 787–790.

Ayers, J. C., and Watson, E. B., 1991, Solubility of apatite, monazite, zircon, and rutile in supercritical aqueous fluids with implications for subduction zone geochemistry: Philosophical Transactions Royal Society London, ser. A, v. 335, p. 365–375.

Ayers, J. C., and Watson, E. B., 1993, Rutile solubility and mobility in supercritical aqueous fluids: Contributions to Mineralogy and Petrology, v. 114, p. 321–330.

Bohlen, S. R., Wall, V. J., and Boettcher, A. L., 1983, Experimental investigations and geologic applications of equilibria in the system FeO-TiO_2-Al_2O_3-SiO_2-H_2O, American Mineralogist, v. 68, p. 1049–1058

Bucher, K., and Frey, M., 1994, Petrogenesis of metamorphic rocks: Berlin, Springer, 318 p.

Cowan, D. S., and Brandon, M. T., 1994, A symmetry-based method for kinematic analysis of large-slip brittle fault zones: American Journal of Science, v. 294, p. 257–306.

Dodson, M. H., Cavanagh, B. J., Thatcher, E. C., and Aftalion, M., 1975, Age limits for the Ubendian metamorphic episode in northern Malawi: Geological Magazine, v. 112, p. 403–410.

England, P. C., and Molnar, P., 1993, The interpretation of inverted metamorphic isograds using simple physical calculations: Tectonics, v. 12, p. 145–158.

England, P. C., and Thompson, A. B., 1984, Pressure-temperature-time paths of regional metamorphism. I. Heat transfer during the evolution of regions of thickened continental crust: Journal of Petrology, v. 25, p. 894–928.

Etheridge, M. A., 1983, Differential stress magnitudes during regional deformation and metamorphism: Upper bound imposed by tensile fracturing: Geology, v. 11, p. 231–234.

Fitches, W. R., 1970, A part of the Ubendian orogenic belt in northern Malawi and Zambia: Geologische Rundschau, v. 59, p. 444–457.

Flinn, D., 1962, On folding during three dimensional progressive deformation: Quaternary Journal of the Geological Society London, v. 118, p. 385–433.

Flöttmann, T., 1988, Strukturentwicklung, P-T-Pfade und Deformationsprozesse im zentralschwarzwälder Gneiskomplex: Frankfurter geowissenschaftliche Arbeiten, v. 6, p. 1–206.

Gaskell, J. L., 1973, The geology of the Mzimba area: Geological Survey Department Bulletin, v. 37, p. 1–30.

Ghosh, S. K., and Ramberg, H., 1976, Reorientation of inclusions by combination of pure shear and simple shear: Tectonophysics, v. 34, p. 1–70.

Graham, M. C., and Powell, R., 1984, A garnet-hornblende geothermometer: Calibration, testing, and application to the Pelona Schist, southern California: Journal of Metamorphic Geology, v. 2, p. 13–31.
Grant, J. A., 1986, The isocon diagram—A simple solution to Gresens's equation for metasomatic alteration: Economic Geology, v. 81, p. 1976–1982.
Gresens, R. L., 1967, Composition-volume relationships of metasomatism: Chemical Geology, v. 2, p. 47–65.
Hubbert, M. K., and Rubey, W. W., 1959, Role of fluid pressure in overthrust faulting: Geological Society of America Bulletin, v. 70, p. 115–168.
Jeffery, G. B., 1922, The motion of ellipsoidal particles immersed in a viscous fluid: Proceedings of the Royal Society of London, ser. A, v. 102, p. 161–179.
Kamb, W. B., 1959, Ice petrofabric observations from Blue Glacier, Washington, in relation to theory and experiment: Journal of Geophysical Research, v. 64, p. 1891–1909.
Kohn, M. J., and Spear, F. S., 1989, Empirical calibration of geobarometers for the assemblage garnet + hornblende + plagioclase + quartz: American Mineralogist, v. 74, p. 77–84.
Kohn, M. J., Orange, D. L., Spear, F. S., Ruble, D., and Harrison, T. M., 1992, Pressure, temperature, and structural evolution of west-central New Hampshire: Hot thrust over cold basement: Journal of Petrology, v. 33, p. 521–556.
Law, R. D., Knipe, R. J., and Dayan, H., 1984, Strain path partitioning within thrust sheets: Microstructural and petrofabric evidence from the Moine thrust zone at Loch Eriboll, northwest Scotland: Journal of Structural Geology, v. 6, p. 477–497.
Losert, J., 1968, On the genesis of nodular sillimanitic rocks: International Geological Congress, 12th, Proceedings, v. 4, p. 109–122.
Means, W. D., Hobbs, B. E., Lister, G. S., and Williams, P. F., 1980, Vorticity and non-coaxiality in progressive deformation: Journal of Structural Geology, v. 2, p. 371–378.
Mott, N. F., 1948, Slip at grain boundaries and grain growth in metals: Proceedings of the Physical Society of London, v. 60, p. 391–394.
Murrell, S. A. F., 1985, Aspects of relationships between deformation and prograde metamorphism that causes evolution of water, *in* Thompson, A. B., and Rubie, D. C., eds., Advances in physical geochemistry 4: Metamorphic reactions, kinetics, textures and deformation: Berlin, Springer, p. 221–241.
Newman, J., and Mitra, G., 1993, Lateral variations in mylonite zone thickness as influenced by fluid-rock interactions, Linville Falls fault, North Carolina: Journal of Structural Geology, v. 15, p. 849–863.
O'Hara, K. D., 1988, Fluid flow and volume loss during mylonitization: An origin for phyllonite in an overthrust setting: Tectonophysics, v. 156, p. 21–34.
O'Hara, K. D., 1990, State of strain in mylonites from the western Blue Ridge province, southern Appalachians: The role of volume loss: Journal of Structural Geology, v. 15, p. 849–863.
O'Hara, K. D., 1994, Fluid-rock interaction in crustal shear zones: A directed percolation approach: Geology, v. 22, p. 843–846.
O'Hara, K. D., and Blackburn, W. H., 1990, Volume-loss model for trace-element enrichments in mylonites: Geology, v. 18, p. 524–527.
Passchier, C. W., 1987, Stable positions of rigid objects in noncoaxial flow: A study in vorticity analysis: Journal of Structural Geology, v. 9, p. 679–690.
Passchier, C. W., 1988, Analysis of deformation paths in shear zones: Geologische Rundschau, v. 77, p. 309–318.
Passchier, C. W., 1997, The fabric attractor: Journal of Structural Geology, v. 19, p. 113–127.
Passchier, C. W., and Trouw, R. A. J., 1996, Microtectonics: Berlin, Springer, 289 p.
Pfiffner, O. A., and Ramsay, J. G., 1982, Constraints on geological strain rates—Arguments from finite strain states of naturally deformed rocks: Journal of Geophysical Research, v. 87, p. 311–321.
Raj, R., and Chung, C. K., 1981, Solution-precipitation creep in glass ceramics: Acta Metallurgica, v. 29, p. 159–166.
Ray, G. E., 1975, The geology of the Chitipa-Karonga area: Geological Survey Department Bulletin, v. 42, p. 1–101.
Ring, U., 1993, Aspects of the kinematic history and mechanism of superposition of the Proterozoic mobile belts of eastern Central Africa (northern Malawi and southern Tanzania): Precambrian Research, v. 61, p. 207–226.
Ring, U., 1997, Volume strain, strain type and flow path in a narrow shear zone: Geologische Rundschau, v. 86, p. 786–801.
Ring, U., Kröner, A., and Toulkeridis, T., 1997, Palaeoproterozoic granulite-facies metamorphism and granitic intrusions in the Ubendian-Usagaran Orogen of northern Malawi, east-central Africa: Precambrian Research, v. 85, p. 27–51.
Robin, P.-Y. F., and Cruden, A. R., 1994, Strain and vorticity patterns in ideally ductile transpression zones: Journal of Structural Geology, v. 16, p. 447–466.
Selverstone, J., Morteani, G., and Staude, J.-M., 1991, Fluid channeling during ductile shearing: Transformation of granodiorite into aluminous schist in the Tauern Window, Eastern Alps: Journal of Metamorphic Geology, v. 9, p. 419–431.
Simpson, C., and De Poar, D. G., 1993, Strain and kinematic analysis in general shear zones: Journal of Structural Geology, v. 15, p. 1–20.
Stern, W. B., 1972, Zur röntgenspektrometrischen Analyse von silikatischen Gesteinen und Mineralien: Schweizerische Mineralogische und Petrographische Mitteilungen, v. 52, p. 1–25.
Underwood, E. E., 1970, Quantitative stereology: Reading, Pennsylvania, Addison-Wesley, 274 p.
Vernon, R. H., 1976, Metamorphic processes, London, Allen and Unwin, 247 p.
Vernon, R. H., and Flood, R. H., 1976, Interpretation of metamorphic assemblages containing fibrolitic sillimanite: Contributions to Mineralogy and Petrology, v. 59, p. 227–235.
Walter, J. V., and Helgeson, H. C., 1977, Calculation of the thermodynamic properties of aqueous silica and the solubility of quartz and its polymorphs at high pressures and temperatures: American Journal of Science, v. 277, p. 1315–1351.
White, S. H., and Knipe, R. J., 1978, Transformation- and reaction-enhanced ductility in rocks: Journal Geological Society of London, v. 135, p. 513–516.
Wintsch, R. P., 1985, The possible effects of deformation on chemical processes in metamorphic fault zones, *in* Thompson, A. B., and Rubie, D. C., eds., Advances in physical geochemistry 4: Metamorphic reactions, kinetics, textures and deformation: Berlin, Springer, p. 251–268.
Zwart, H. J., 1965, Geological map of the Paleozoic of the Central Pyrenees (Sheet 6, Aston, France, Andorra, Spain, 1: 50 000): Leidse geologische Medelingen, v. 33, p. 191–254.

MANUSCRIPT RECEIVED BY THE SOCIETY JUNE 29, 1997
REVISED MANUSCRIPT RECEIVED JANUARY 5, 1998
MANUSCRIPT ACCEPTED MARCH 18, 1998

Printed in U.S.A.